



1 **Volatility and lifetime against OH heterogeneous reaction of ambient Isoprene Epoxydiols-**
2 **Derived Secondary Organic Aerosol (IEPOX-SOA)**

3 Weiwei Hu^{1,2}, Brett B. Palm^{1,2}, Douglas A. Day^{1,2}, Pedro Campuzano-Jost^{1,2}, Jordan E.
4 Krechmer^{1,2}, Zhe Peng^{1,2}, Suzane S. de Sá³, Scot T. Martin^{3,4}, M. Elizabeth Alexander⁵, Karsten
5 Baumann⁶, Lina Hacker⁷, Astrid Kiendler-Scharr⁷, Abigail R. Koss^{1,2,8}, Joost A. de Gouw^{1,2,8},
6 Allen H. Goldstein^{9,10}, Roger Seco¹¹, Steven J. Sjostedt⁸, Jeong-Hoo Park¹², Alex B. Guenther¹¹,
7 Saewung Kim¹¹, Francesco Canonaco¹³, André. S. H. Prévôt¹³, William H. Brune¹⁴, Jose L.
8 Jimenez^{1,2}

9 1 Cooperative Institute for Research in Environmental Sciences, University of Colorado,
10 Boulder, CO, USA 80309
11 2 Department of Chemistry and Biochemistry, University of Colorado, Boulder, CO, USA 80309
12 3 John A. Paulson School of Engineering and Applied Sciences Harvard University, Cambridge,
13 MA, USA 01742
14 4 Department of Earth and Planetary Sciences, Harvard University, Cambridge, MA, USA 01742
15 5 Environmental Molecular Sciences Laboratory, Pacific Northwest National Laboratory,
16 Richland, WA, USA 99352
17 6 Atmospheric Research and Analysis Inc., Morrisville, NC, USA 27560
18 7 Institute for Energy and Climate Research - Troposphere (IEK-8), Forschungszentrum Jülich,
19 D-52425 Jülich, German
20 8 Earth System Research Laboratory, NOAA, Boulder, Colorado, USA 80305
21 9 Department of Environmental Science, Policy, and Management, University of California,
22 Berkeley, CA, USA 94720
23 10 Department of Civil and Environmental Engineering, University of California, Berkeley, CA,
24 USA 94720
25 11 Department of Earth System Science, University of California, Irvine, USA 92697
26 12 National Institute of Environmental Research, Republic of Korea 22689
27 13 Laboratory of Atmospheric Chemistry, Paul Scherrer Institute (PSI), 5232 Villigen,
28 Switzerland
29 14 Department of Meteorology, Pennsylvania State University, University Park, PA, USA 16802
30 Correspondence to: J. L. Jimenez (jose.jimenez@colorado.edu)

31 **Abstract**

32 Isoprene epoxydiols-derived secondary organic aerosol (IEPOX-SOA) can contribute
33 substantially to organic aerosol (OA) concentrations in forested areas under low NO conditions,
34 hence significantly influencing the regional and global OA budgets, accounting for example for
35 16-36% of the submicron OA in the SE US summer. Particle evaporation measurements from a
36 thermodenuder show that the volatility of ambient IEPOX-SOA is lower than that of bulk OA
37 and also much lower than that of known monomer IEPOX-SOA tracer species, indicating that
38 IEPOX-SOA likely exists mostly as oligomers in the aerosol phase. The OH aging process of
39 ambient IEPOX-SOA was investigated with an oxidation flow reactor (OFR). New IEPOX-SOA
40 formation in the reactor was negligible, as the OFR cannot accelerate processes such as aerosol
41 uptake and reactions that do not scale with OH. Simulation results indicate that adding ~100 μg
42 m^{-3} of pure H_2SO_4 to the ambient air allows to efficiently form IEPOX-SOA in the reactor. The



43 heterogeneous reaction rate coefficient of ambient IEPOX-SOA with OH radical (k_{OH}) was
44 estimated as $4.0 \pm 2.0 \times 10^{-13} \text{ cm}^3 \text{ molec}^{-1} \text{ s}^{-1}$, which is equivalent to more than a 2-week lifetime.
45 A similar k_{OH} was found for measurements of OH oxidation of ambient Amazon forest air in an
46 OFR. At higher OH exposures in the reactor ($>1 \times 10^{12} \text{ molec. cm}^{-3} \text{ s}$), the mass loss of IEPOX-
47 SOA due to heterogeneous reaction was mainly due to revolatilization of fragmented reaction
48 products. We report for the first time OH reactive uptake coefficients ($\gamma_{OH}=0.59 \pm 0.33$ in SE US
49 and $\gamma_{OH}=0.68 \pm 0.38$ in Amazon) for SOA under ambient conditions. A relative humidity
50 dependence of k_{OH} and γ_{OH} was observed, consistent with surface area-limited OH uptake. No
51 decrease of k_{OH} was observed as OH concentrations increased. These observation of
52 physicochemical properties of IEPOX-SOA can help to constrain OA impact on air quality and
53 climate.

54



55 **1 Introduction**

56 Organic aerosol (OA), which comprises 10-90% of ambient submicron aerosol mass
57 globally, has important impacts on climate forcing and human health (Kanakidou et al., 2005;
58 Zhang et al., 2007; Hallquist et al., 2009). However, quantitative predictions of OA mass
59 concentrations often fails to match the real ambient measurements by large factors,
60 (e.g. Volkamer et al., 2006; Dzepina et al., 2011; Tsigaridis et al., 2014). Improved
61 characterization of the properties and lifetime of OA is needed to better constrain OA model
62 predictions.

63 Isoprene is the most abundant non-methane hydrocarbon (NMHC) emitted into the Earth's
64 atmosphere (Guenther et al., 2012). Many studies in the past decade have shown that the reaction
65 products of isoprene-derived epoxydiols (IEPOX), formed under low NO conditions (Paulot et
66 al., 2009), can contribute efficiently to secondary OA (SOA) via reactive uptake of gas-phase
67 IEPOX onto acidic aerosols (Eddingsaas et al., 2010; Froyd et al., 2010; Surratt et al., 2010; Lin
68 et al., 2012; Liao et al., 2015). IEPOX-SOA measurements in field studies show that it can
69 account for 6-34% of total OA over multiple forested areas across the globe, with important
70 impacts on the global and regional OA budget (Hu et al., 2015). Although the formation of
71 IEPOX-SOA from gas-phase IEPOX has been investigated in many laboratory studies (e.g.
72 Eddingsaas et al., 2010; Lin et al., 2012; Gaston et al., 2014), the lifetime and aging of IEPOX-
73 SOA in the aerosol phase is still mostly unexplored in the literature.

74 IEPOX-SOA can be measured by multiple methods. Gas chromatography/mass
75 spectrometry (GC/MS) or liquid chromatography/mass spectrometry (LC/MS) of filter extracts
76 can be used to measure some IEPOX-SOA species (accounting for 8-80% of total IEPOX-SOA
77 depending on the study, Lin et al., 2012; Budisulistiorini et al., 2015; Hu et al., 2015). Recently,
78 several studies have shown that factor analysis of real-time aerosol mass spectrometer (AMS)
79 data provides a method to obtain the total amount, overall fraction contribution, and properties of
80 IEPOX-SOA (Robinson et al., 2011; Budisulistiorini et al., 2013; Chen et al., 2015). The $C_5H_6O^+$
81 ion at m/z 82 in AMS spectra, arising from decomposition and ionization of molecular IEPOX-
82 SOA species, has also been suggested as a proxy for real-time estimation of IEPOX-SOA (Hu et
83 al., 2015).



84 Heterogeneous reaction of OA with hydroxyl radicals (OH) is a contributor to aerosol
85 aging and significantly influences aerosol lifetime (George and Abbatt, 2010; George et al.,
86 2015). To describe the aging process, OA reaction rate coefficients with OH radicals (k_{OH}), or
87 alternatively uptake coefficients of OH (γ_{OH}), defined as the fraction of OH collisions with a
88 compound that result in reaction, have been reported for numerous laboratory studies. Values of
89 effective γ_{OH} (≤ 0.01 to ≥ 1) also can vary significantly under different reaction conditions, such
90 as different OA species (George and Abbatt, 2010), temperature and humidity (Park et al., 2008;
91 Liu et al., 2012; Slade and Knopf, 2014), OH concentrations (Slade and Knopf, 2013; Arangio et
92 al., 2015), and particle phase state or coatings (McNeill et al., 2008; Arangio et al., 2015). Most
93 of the studies that have reported k_{OH} and γ_{OH} are based on laboratory experiments, with few
94 experimental determinations of k_{OH} based on field measurements under ambient conditions
95 (Slowik et al., 2012; Ortega et al., 2015), while no γ_{OH} has been reported based on field studies to
96 our knowledge.

97 During the Southern Oxidant and Aerosol Study (SOAS), 17% of ambient OA was
98 estimated to be IEPOX-SOA (Hu et al., 2015). In this study, ambient gas and aerosol species
99 were sampled through an oxidation flow reactor (OFR) and a thermodenuder (TD) to investigate
100 heterogeneous oxidation and evaporation of ambient IEPOX-SOA, respectively. These systems
101 included an AMS and other on-line instruments measuring both gas and aerosol species inflow
102 and outflow. A simplified box model is used to investigate the fate of gas-phase IEPOX under
103 ambient and OFR conditions. The potential of evaporation to impact the lifetime of IEPOX-SOA
104 was evaluated. The heterogeneous reaction rate coefficient (k_{OH}) and OH uptake coefficient (γ_{OH})
105 of IEPOX-SOA with OH radicals are estimated from the OFR data. IEPOX-SOA aging during
106 the dry season of 2014 in central Amazonia as part of the Green Ocean Amazon
107 (GoAmazon2014/5, IOP2) experiment, using the same OFR experimental setup, was compared
108 to the SOAS results.

109 2 Experimental method

110 2.1 Background and instrumentation

111 The SOAS study (hereafter refer to “SE US study”) took place in the SE US in the summer
112 (June 1– July 15) of 2013. Results shown here are from the SEARCH Centreville Supersite
113 (CTR) in a mixed forest in Alabama (32.95° N, 87.13°W; Hansen et al., 2003). The average



114 (\pm standard deviation) temperature and relative humidity (RH) of ambient air were $25\pm 4^\circ\text{C}$ and
115 $83\pm 18\%$, respectively (Fig. S1). Biogenic volatile organic compounds (BVOCs) were highly
116 abundant with average isoprene and monoterpene concentrations of 3.3 ± 2.4 ppb and 0.7 ± 0.4
117 ppb, respectively, and they displayed clear diurnal variations (Fig. S1). Isoprene showed a broad
118 mid-afternoon peak (~ 5.8 ppb), and monoterpenes peaked during the nighttime and early
119 morning (~ 0.9 - 1.0 ppb). Chemically-resolved mass concentrations of submicron non-refractory
120 aerosol (PM_{10}) were measured by a high-resolution time-of-flight AMS (HR-ToF-AMS,
121 Aerodyne Research Inc., DeCarlo et al., 2006) at a time resolution of 2 min. Detailed information
122 about AMS setup, operation and data analysis is given in the supporting information and as well
123 as in Hu et al. (2015).

124 A “Potential Aerosol Mass” oxidation flow reactor (OFR) was used to investigate OA
125 formation/aging from ambient air over a wide range of OH exposures (10^{10} - 10^{13} molec. cm^{-3} s).
126 This field-deployable OFR provides a fast and direct way to investigate oxidation processes of
127 ambient gas and aerosol with OH radicals under low-NO chemistry (Kang et al., 2007; Lambe et
128 al., 2011; Li et al., 2015a; Ortega et al., 2015; Peng et al., 2015b; Palm et al., 2016). The OFR is
129 a cylindrical vessel (~ 13 L) with an average residence time of ~ 180 - 220 s in this study,
130 depending on the flow rates of sampled ambient air (3.5 - 4.2 L min^{-1}) (Fig. S2-S3). In the
131 “OFR185” method of OH production used in this study, two low-pressure mercury lamps inside
132 the OFR produce UV radiation at 185 and 254 nm (Peng et al., 2015b). OH radicals were
133 generated when the UV light initiated O_2 , H_2O , and O_3 photochemistry (Li et al., 2015a). A large
134 range of OH exposures (10^{10} - 10^{13} molec. cm^{-3} s) can be achieved by varying UV light intensity,
135 equivalent to several hours to several weeks of photochemical aging of ambient air (assuming a
136 24-hr average $\text{OH} = 1.5 \times 10^6$ molec. cm^{-3} ; Mao et al., 2009). OH exposures in the OFR were
137 calculated by the real-time decay of CO added to the ambient air in the OFR (1-2 ppm; OH
138 reactivity ≈ 5 - 10 s^{-1}). OH exposures in the OFR were calculated by the real-time decay of CO
139 added to the ambient air in the OFR (1-2 ppm; OH reactivity ≈ 5 - 10 s^{-1}). The empirical estimation
140 of OH exposure based on the OFR output parameters O_3 , water, and ambient OH reactivity (15
141 s^{-1}) showed good agreement with that calculated from CO decay as shown in Fig. S4 (2015a).
142 The uncertainty of calculated OH exposures in the OFR was estimated as 35% based on
143 regression analysis (Li et al., 2015a; Peng et al., 2015b).



144 The average wall loss corrections for OA in OFR during the SE US study is $2\pm 0.7\%$. This
145 wall loss is estimated by comparing the ambient OA concentrations to those concentrations after
146 the OFR when the UV lights were off and no oxidant was present (other than ambient O_3).

147 A TD was used to investigate the volatility of ambient OA and IEPOX-SOA. The
148 temperature in the TD increased linearly during the heating period (from 30°C to 250°C over 60
149 min) and then cooled down to 30°C for 60 min. More detailed information on the TD technique
150 and instrumentation can be obtained elsewhere (Faulhaber et al., 2009; Huffman et al., 2009a;
151 Huffman et al., 2009b).

152 A typical sampling cycle during SE US study took a total of 24 min, sequentially sampling
153 ambient (4 min), TD (4 min), ambient (4 min), OFR with OH radicals as oxidant (4 min),
154 ambient (4 min), and OFR with other types of oxidation (e.g., O_3 or NO_3 as oxidants; 4 min), as
155 illustrated in the diagram in Fig. S2. Only OFR data for OH oxidation using OFR 185 method is
156 presented here. UV light intensities in the OFR were changed immediately after sampling the
157 second OFR outflow for each cycle. Thus, oxidant concentrations in the OFR had sufficient time
158 (at least 12 min, i.e. 3-4 flow e-folding times) to stabilize before the next OFR sampling interval.
159 The air from each sampling mode was sampled by the AMS, a scanning mobility particle sizer
160 (for measuring particle number size distributions; SMPS, TSI Inc.), and several other instruments
161 to measure related gas phase species, e.g., VOCs from proton-transfer-reaction mass
162 spectrometer (PTR-MS), O_3 , CO and H_2O (Table S1).

163 Measurements collected during the second Intensive Operating Period (IOP2) of the Green
164 Ocean Amazon (GoAmazon2014/5, hereinafter “Amazon study”) Experiment (Martin et al.,
165 2015), which took place in the dry season of central Amazonia, are also presented here. The
166 region has high isoprene and monoterpene emissions (Karl et al., 2007; Martin et al., 2010). In
167 this analysis, data from the “T3” ground site (3.213°S , 60.599°W), a rural location 60 km west of
168 Manaus (Pop. 2 million) in the dry season (Aug. 15 to Oct. 15, 2014) are also shown. Unlike SE
169 US study, the aerosols in dry season of Amazon study were heavily influenced by biomass
170 burning, thus providing a difference dataset to investigate IEPOX-SOA heterogeneous reaction.
171 The instrument setup, OFR settings, sampling schemes and data processing were similar to those
172 for SE US study.

173 **2.2 IEPOX-SOA identification**



174 We classified ambient OA using positive matrix factorization (PMF) on the time series of
175 peak-fitted, high-resolution organic spectra measured by the AMS (Ulbrich et al., 2009). A factor
176 corresponding to ambient IEPOX-SOA was assigned based on its spectral features (e.g.
177 prominent $C_5H_6O^+$ ion at m/z 82), and strong correlation with hourly or daily-measured 2-
178 methyltetrols ($R=0.79$), an oxidation product of isoprene oxidation via the IEPOX pathway
179 (Surratt et al., 2010; Hu et al., 2015), as well as with sulfate ($R=0.75$), which facilitates IEPOX-
180 SOA formation through direct reactions or nucleophilic effects (Nguyen et al., 2014a; Liao et al.,
181 2015). Unconstrained PMF analysis often fails when the factor fractions become too small
182 ($<5\%$), e.g., as is for the IEPOX-SOA at higher OH exposures in the OFR in this study (Ulbrich
183 et al., 2009). To overcome this, a more advanced algorithm, the Multilinear Engine (ME-2)
184 (Paatero, 2007; Canonaco et al., 2013), was applied through the recently implemented Source
185 Finder (SoFi, Canonaco et al., 2013). In SoFi, the mass spectrum of the IEPOX-SOA factor was
186 constrained based on the ambient spectrum of IEPOX-SOA from conventional PMF, and the
187 concentrations of IEPOX-SOA factors were retrievable even at low concentrations. More
188 information can be found in Supp. Info. (Sect. 2 and Fig. S5-S9). Here after we will call IEPOX-
189 SOA PMF factor to be IEPOX-SOA for abbreviation.

190 In this study, $C_5H_6O^+$ data directly measured from AMS is used as a complementary tool to
191 examine/interpret the analysis results from IEPOX-SOA PMF factor, since both lab and ambient
192 results have shown $C_5H_6O^+$ is a very good tracer for IEPOX-SOA (Hu et al., 2015). Analyzing
193 $C_5H_6O^+$ is an easy alternative method to evaluate the physicochemical evolution of IEPOX-SOA,
194 that avoids the uncertainties related to PMF analysis, and thus provides further confidence in the
195 results. This is especially true when periods where the OA is dominated by IEPOX-SOA are
196 analyzed.

197 **2.3 Box model to simulate gas-phase IEPOX**

198 The chemistry of OH oxidation in the OFR is typical of low-NO conditions with HO_2 being
199 the dominant reaction partner of RO_2 radicals due to the greatly elevated HO_2 concentrations and
200 the very short lifetime of NO and NO_x in OFR (Li et al., 2015a; Peng et al., 2015b). A box model
201 (KinSim 3.2 in Igor Pro. 6.37) was used to simulate the fate of gas-phase IEPOX under both
202 ambient and OFR conditions, as shown in Fig. 3 (Paulot et al., 2009; Xie et al., 2013; Bates et
203 al., 2014; Krechmer et al., 2015). A detailed description, including reactions and parameters in
204 the model, pH-dependent uptake coefficient of IEPOX onto aerosols (γ_{IEPOX}), aerosol surface



205 area calculations and estimated photolysis of IEPOX, can be found in Supp. Info. Section 3
206 (Table S2-3 and Fig. S10-14).

207 **3 Results and discussion**

208 **3.1 Low Volatility of IEPOX-SOA**

209 TDs are widely used to investigate the volatility distribution of OA in ambient air (e.g.
210 Faulhaber et al., 2009; Cappa and Jimenez, 2010). IEPOX-SOA evaporates more slowly upon
211 heating (Fig. 1a) than total OA over a very wide range of TD temperatures (<170°C), indicating
212 that IEPOX-SOA has a lower volatility than bulk OA. Consistent with that result, a lower
213 volatility of the IEPOX-SOA tracer $C_5H_6O^+$ in both SE US and Amazon studies was also found
214 (Fig. 2).

215 The volatility distributions of IEPOX-SOA and OA were estimated following the method of
216 Faulhaber et al. (2009), based on calibration of the relationship between TD temperature and
217 organic species saturation concentration at 298 K (C^*). Similar methods have been developed for
218 other thermal desorption instruments (e.g., Chattopadhyay and Ziemann, 2005; Lopez-Hilfiker et
219 al., 2016). The volatility distribution of IEPOX-SOA (Fig. 1b) shows mass peaks at $C^*=10^{-4}$ –
220 $10^{-3} \mu\text{g m}^{-3}$, which are much lower than those of diesel POA ($C^*=10^{-2}$ – $1 \mu\text{g m}^{-3}$) and biomass-
221 burning POA ($C^*=10^{-2}$ – $100 \mu\text{g m}^{-3}$, Fig. 1d) at various OA concentrations (1 – $100 \mu\text{g m}^{-3}$). Those
222 types of OA are reported to be semivolatile (Cappa and Jimenez, 2010; Ranjan et al., 2012; May
223 et al., 2013). The estimated distribution implies that very little of the ambient IEPOX-SOA was
224 actively partitioning to the gas phase during SE US study (Fig. 1b). Although we cannot rule out
225 some chemical changes during TD heating, this conclusion is dictated by the data at the lowest
226 TD temperatures, when such chemistry is less likely. Lopez-Hilfiker et al. (2016) have shown
227 that oligomer decomposition for IEPOX-SOA upon heating at $\sim 90^\circ\text{C}$ was important during SE
228 US study, but that process will only make the measured volatility of IEPOX-SOA in TD higher
229 than it should be. This reinforces our conclusion about the low volatility of ambient IEPOX-
230 SOA, consistent with the independent results of Lopez-Hilfiker et al. (2016).

231 Several molecular species (e.g., 2-methyltetrols, C_5 -alkene triols, IEPOX organosulfate and
232 its dimer) comprising IEPOX-SOA have been characterized both in field and chamber studies
233 (Surratt et al., 2010; Lin et al., 2012; Budisulistiorini et al., 2013; Liao et al., 2015). At the CTR
234 site during the SE US study, 2-methyltetrols, C_5 -alkene triols and IEPOX organosulfate



235 measured by GC/MS and LC/MS in the particle phase accounted for an average of 80%
236 (individually 29%, 28% and 24%, respectively) of total IEPOX-SOA factor mass (Hu et al.,
237 2015). The volatilities of these IEPOX-SOA molecular species was estimated based on SIMPOL
238 group contribution method (Pankow and Asher, 2008). The species reported to comprise most of
239 IEPOX-SOA have relatively high C^* (2-methyltetrol= $2.7 \mu\text{g m}^{-3}$; C_5 -alkene triols= $400 \mu\text{g m}^{-3}$,
240 and IEPOX organosulfate= $0.5 \mu\text{g m}^{-3}$). The alkene triols in ambient air during SE US study
241 (where average OA mass concentration was $4.8 \mu\text{g m}^{-3}$) should have been almost completely in
242 the gas phase (>98%), while 36% and 10% of the methyltetrol and organosulfate should have
243 been in the gas-phase, respectively. The C^* of those monomer species is much higher than for
244 the bulk IEPOX-SOA ($C^*=10^{-6}$ – $10^{-2} \mu\text{g m}^{-3}$) that they are thought to comprise. On the other
245 hand, the estimated C^* of a hypothetical methyltetrol molecular dimer ($\sim 10^{-7} \mu\text{g m}^{-3}$) is
246 significantly lower than that of most of the bulk IEPOX-SOA (Fig. 1d). This suggests that
247 IEPOX-SOA may exist as oligomers in the aerosol phase, but that the oligomers were not
248 evaporating as oligomers, rather decomposing and evaporating as monomer species at
249 temperatures intermediate with those corresponding to the C^* of the monomers and the dimers,
250 consistent with results of Lopez-Hilfiker et al. (2016).

251 Further evidence supporting low volatility and strong oligomerization of IEPOX-SOA
252 molecular species has also been reported. Lin et al. (2014) showed oligomers as part of IEPOX-
253 SOA in filter-based LC/MS measurement at three sites (including CTR) during SE US study.
254 Some of the oligomers were separated by mass units of 100 ($\text{C}_5\text{H}_8\text{O}_2$) and 82 ($\text{C}_5\text{H}_6\text{O}$), which
255 would be consistent with C_5 -alkene triol ($\text{C}_5\text{H}_{10}\text{O}_3$) and methyltetrol ($\text{C}_5\text{H}_{12}\text{O}_4$) oligomerization
256 though dehydration reactions ($-\text{H}_2\text{O}$ or $2 \text{H}_2\text{O}$), or with other reactions resulting in similar
257 products. Results from online gas-particle partitioning measurements at the same site during this
258 study have shown that the measured particle-phase fractions (F_p , negatively correlated with C^*)
259 of ambient IEPOX-SOA tracers (e.g., 2-methyltetrols and C_5 -alkene triols) are much higher than
260 expected based on the species vapor pressures, consistent with these tracers being formed during
261 GC analysis by decomposition of larger molecules (likely oligomers) (Isaacman-VanWertz et al.,
262 2016). Thus, the low volatility of IEPOX-SOA estimated from our TD data is consistent with
263 multiple other measurements.



264 Using the volatility distributions determined from the TD, the fractional losses for both OA
265 and IEPOX-SOA due to evaporation upon dilution can be estimated. This parameter can be
266 quantified as (Cappa and Jimenez, 2010):

$$267 \quad E_{loss} = 100\% \left[1 - \frac{C_{OA}(DF)}{C_{OA}(0)/DF} \right] \quad (1)$$

268 where E_{loss} is the fractional OA loss due to evaporation; $C_{OA}(0)$ is the initial organic mass
269 concentration before dilution, and DF is the dilution factor applied. $C_{OA}(DF)$ is the OA
270 concentration in equilibrium after dilution. Dilution factors varying from one to thirty were used
271 here. The results are shown in Fig. 1c. After a 30-fold dilution, IEPOX-SOA mass loss due to
272 evaporation is estimated to be ~5%, substantially lower than for total OA (17%). There are two
273 uncertainties affecting this result. One is that the real volatility distribution of IEPOX-SOA is
274 likely even lower, since the TD results are thought to be affected by oligomer decomposition
275 upon heating. The other one is that this calculation neglects the effect of possible decomposition
276 of oligomers onto monomers in ambient air. If that process occurs on a timescale of e.g., 1day, it
277 would lead to higher evaporated fractions than estimated here. The residence time of TD is
278 ~10-15s, which may not be sufficient time for oligomer decomposition, especially at the lower
279 temperatures that determined the upper end of the estimated volatility distribution. E.g. Vaden et
280 al (2011) reported that it took 24 h to evaporate 75% of α -pinene SOA. The kinetics of oligomer
281 decomposition of IEPOX-SOA under ambient conditions should be further investigated to fully
282 constrain its evaporation dynamics.

283 3.2 Fate of gas-phase IEPOX

284 IEPOX-SOA loadings exhibited a continuous decrease as OH exposure increases in the
285 OFR. To interpret the observed decay of IEPOX-SOA in the OFR, we first need to understand
286 whether additional IEPOX-SOA was formed in the OFR during SE US study. More details about
287 the IEPOX-SOA decay will be discussed in Sect. 3.3. Here, the box model described above (Fig.
288 3) was used to simulate the fate of gas-phase IEPOX in OFR and ambient conditions, as shown
289 in Fig. 4.

290 In ambient air, gas-phase IEPOX will either react with OH radicals to form more oxidized
291 gas-phase products (e.g. hydroxyacetone) (Bates et al., 2014; Bates et al., 2015), be taken up
292 onto acidic aerosol (Surratt et al., 2010), or be lost from the atmosphere by dry or wet deposition
293 (Nguyen et al., 2015). Photolysis of IEPOX in ambient air should be negligible, since the



294 epoxide and hydroxyl groups in IEPOX are photostable at visible or actinic UV wavelengths
295 (Fleming et al., 1959). A model scenario accounting for organic resistance with slower IEPOX
296 uptake than pure inorganic is applied to simulate the fate of gas-phase IEPOX. This scenario is
297 the most realistic assumption, since 67% of ambient aerosol is OA during SE US study (Fig.
298 S15). Results from an alternative model assuming pure inorganic aerosols are shown in Supp.
299 Info. The model predicts that the main pathway of gas-phase IEPOX removal in ambient air is
300 aerosol-phase uptake during SE US study, where about 75% of IEPOX was taken up by the
301 aerosol after one day under ambient conditions, because of the efficient uptake of gas-phase
302 IEPOX onto acidic ambient aerosols ($\text{pH}=0.8\pm 0.5$) at the CTR site ($\gamma_{\text{IEPOX}}=0.009$, lifetime~1.8
303 h). The rest of IEPOX was lost to dry deposition to the surface (16%), according to reported
304 boundary layer of 1200 m and dry deposition rate of 3 cm s^{-1} (Nguyen et al., 2015), or to gas-
305 phase reaction with OH (9%).

306 The fate of IEPOX sampled into the OFR differed from its fate in ambient air. Remaining
307 unreacted and then leaving OFR or destruction in the gas phase completely dominate the fate of
308 IEPOX under OFR conditions (Fig 4b). Negligible amounts of IEPOX (<1%) were taken up into
309 the aerosol phase in the OFR. This is mainly because the lifetime of IEPOX aerosol uptake
310 ($\gamma_{\text{IEPOX}}=0.002$; lifetime=7.0h) was much longer than the OFR residence time (200s). The lower
311 γ_{IEPOX} in OFR (0.002) than in ambient condition (0.008) was because of the higher pH of
312 aerosol leading to a slower IEPOX uptake. Higher pH in OFR (1.35 ± 0.6) than that in ambient
313 (0.8 ± 0.5) was because extra neutralized inorganic aerosol was formed in OFR. Photolysis of
314 IEPOX in OFR is estimated to be very minor (less than 0.2%) (Fig. 4b and Table S3). Loss of
315 IEPOX to the reactor walls is thought to be minor under the conditions of SE US study, given its
316 high vapor pressure (Krechmer et al., 2015; Palm et al., 2016).

317 IEPOX-SOA mass concentrations formed in both ambient and OFR conditions were
318 calculated as a function of OH exposure. For this estimate the molar mass of IEPOX-SOA and
319 the SOA molar yield (φ_{SOA}) of IEPOX, defined as the sum of formed aqueous phase SOA tracer
320 relative to the heterogeneous rate of gas-phase epoxide loss to particles (Riedel et al., 2015), are
321 needed. Using the measured molecular composition of IEPOX-SOA (Hu et al., 2015), and
322 assuming all species were present as dimers as discussed above, yields an average molar mass of
323 bulk IEPOX-SOA of 270 g mol^{-1} . Laboratory uptake experiments showed the SOA molar yield
324 of IEPOX is around 10-12% for acidic NH_4HSO_4 (Riedel et al., 2015). A molar mass of 270 g



325 mol^{-1} and $\phi_{\text{SOA}}=6\%$ (to account for the dimerization) for IEPOX-SOA were applied here. In the
326 OFR, the maximum modeled IEPOX-SOA mass concentrations were less than 12 ng m^{-3} ,
327 peaking at ~ 1 day OH exposure. The model-predicted IEPOX-SOA formation is equivalent to
328 $\sim 1\%$ of the ambient IEPOX-SOA, indicating negligible IEPOX-SOA was formed in the OFR.
329 An upper limit of $\sim 6\%$ of the ambient IEPOX-SOA mass being formed in the OFR can be
330 derived assuming that the particles are 100% inorganic, as shown in Fig. S17.

331 In addition to the box model results, we also have experimental evidence demonstrating
332 negligible IEPOX-SOA formation in the OFR. During the Amazon study, standard additions of
333 isoprene (50-200 ppb) were injected into ambient air at the entrance of the OFR, during a period
334 when little SOA was formed from ambient precursors. After isoprene was exposed to varied OH
335 exposures ($\sim 10^9$ - 10^{12} molec. cm^{-3} s) in the OFR in the presence of ambient aerosols, no
336 additional IEPOX-SOA formation was observed in the oxidized air exiting the OFR, as shown in
337 Fig. 5. Even under optimum OH exposures (8 - 11×10^{10} molec. cm^{-3} s), where most of the
338 isoprene and isoprene hydroperoxide (ISOPOOH) are expected to be oxidized and
339 before substantial decay of IEPOX-SOA occurs, no enhancements of IEPOX-SOA tracer
340 $\text{C}_5\text{H}_6\text{O}^+$ ion abundance in OA spectra were observed. Consistent with our results, a laboratory
341 flow tube study (residence time = 1 min) of low-NO isoprene oxidation in the presence of
342 acidified inorganic seeds also reported negligible IEPOX-SOA formation (Wong et al., 2015).
343 Those results highlight a key limitation of this type of OFR: processes that do not scale with OH
344 and thus are not greatly accelerated in the reactor are not captured. This limitation can be
345 removed by seeding the OFR with H_2SO_4 particles, which greatly accelerate IEPOX aerosol
346 uptake. Simulation results (not shown) indicate that adding $\sim 100 \mu\text{g m}^{-3}$ of pure H_2SO_4 to the
347 ambient air allows to efficiently form IEPOX-SOA in the reactor.

348 **3.3 Lifetime of IEPOX-SOA against OH oxidation**

349 IEPOX-SOA loadings showed a continuous decrease as OH exposure increases in the OFR
350 (Fig. 6a). Since negligible IEPOX-SOA mass was added in the OFR (Sect. 3.2), this decay
351 should be due to the sum of all IEPOX-SOA loss processes. The loss of IEPOX-SOA is defined
352 empirically here as the loss of the molecular structures that result on AMS spectral features of
353 IEPOX-SOA (e.g., $\text{C}_5\text{H}_6\text{O}^+$ and C_4H_5^+ enhancements, Lin et al., 2012; Hu et al., 2015), such that
354 an IEPOX-SOA component cannot be distinguished in constrained PMF analysis. Evaporation,
355 photolysis and heterogeneous reaction with OH radicals are three possible loss pathways.



356 In principle some IEPOX-SOA could evaporate, if semivolatile molecules in equilibrium
 357 with it were oxidized by OH. As discussed above, IEPOX-SOA itself has low volatility and only
 358 a small fraction (~5%) may evaporate to the gas phase after dilution of a factor of 30. Even the
 359 oligomer decomposition could be fast in the ambient air, this process will be negligible in the
 360 flow reactor on a time scale of 3 min. Thus IEPOX-SOA evaporation is unlikely to contribute to
 361 the large observed IEPOX-SOA loss (up to 90%).

362 Photolysis of IEPOX-SOA also cannot explain the large decreases of IEPOX-SOA in Fig.
 363 6a. Washenfelder et al. (2015) reported that IEPOX-SOA during SOAS contributed negligibly to
 364 the aerosol absorption at 365 nm. Lin et al. (2014) reported a wavelength-dependent effective
 365 mass absorption coefficient (MAC) value of ~247 cm² g⁻¹ at 254 nm for laboratory-generated
 366 IEPOX-SOA on acidified NH₄H₂SO₄ seed. Using the MAC trend vs. wavelength and the
 367 measured data down to 200 nm we estimate an MAC of ~5200 cm² g⁻¹ at 185 nm. Using those
 368 absorption efficiencies (and assuming an upper limit quantum yield of 1) we can derive an upper
 369 limit photolysis fraction of 1.5% of IEPOX-SOA in the OFR when neglecting other competing
 370 effects (e.g. OH oxidation, Table S3 and Fig. S18). In addition, the actual quantum yield may be
 371 much less than 1, as IEPOX-SOA molecular species contain mainly hydroxyl and carbonyl
 372 groups (Surratt et al., 2010; Lin et al., 2014). Interactions between these groups are thought to
 373 result in low quantum yields in the condensed phase (Phillips and Smith, 2014; Sharpless and
 374 Blough, 2014; Peng et al., 2015a; Phillips and Smith, 2015). Therefore photolysis of IEPOX-
 375 SOA should contribute negligibly to the observed IEPOX-SOA decay.

376 The observed decay of IEPOX-SOA in Fig. 6a must then be the result of heterogeneous
 377 reactions with OH radicals. This process can be quantitatively described as:

$$378 \quad IEPOX - SOA_i / IEPOX - SOA_0 = e^{-k_{OH} \times OH_i \times \Delta t_i} = e^{-k_{OH} \times OH_{exp,i}} \quad (2)$$

379 where IEPOX-SOA_i is the IEPOX-SOA mass concentration after the *i*th OH exposure step in the
 380 OFR. IEPOX-SOA₀ is the initial ambient IEPOX-SOA entering the OFR; IEPOX-SOA_i/IEPOX-
 381 SOA₀ is the mass fraction remaining of IEPOX-SOA in the OFR output, shown on Fig. 6a. OH_i
 382 is the average OH concentration of step *i* in the OFR, Δ*t*_{*i*} is the photochemical age. OH_{exp,*i*}
 383 = OH_{*i*} × Δ*t*_{*i*} is the OH exposure of step *i*. *k*_{OH} is the heterogeneous reaction rate coefficient
 384 between IEPOX-SOA and OH radicals.

385 Fitting the results in Fig. 6a with Eq. (2) results in a *k*_{OH} of 4.0±2.0×10⁻¹³ cm³ molec.⁻¹ s⁻¹
 386 The 1σ uncertainty was obtained by Monte Carlo simulation, from propagation of the errors of



387 IEPOX-SOA_i/IEPOX-SOA₀ (9%) and the uncertainty of OH exposure (35%, Fig. S4). The
388 uncertainty of IEPOX-SOA_i/IEPOX-SOA₀ was estimated as 9% from PMF analysis of OFR data
389 (Hu et al., 2015).

390 A similar k_{OH} value ($4.6 \times 10^{-13} \text{ cm}^3 \text{ molec.}^{-1} \text{ s}^{-1}$) was obtained by fitting the IEPOX-SOA
391 tracer $\text{C}_3\text{H}_6\text{O}^+$ ion decay as a function of OH exposure during a period (June 26th, 14:00-19:00)
392 when 80-90% of ambient OA was composed of IEPOX-SOA (Fig. S19-S20), which confirms the
393 k_{OH} determined above.

394 For comparison, the average mass fraction remaining of IEPOX-SOA vs. OH exposure
395 during the Amazon study is also shown in Fig. 6a. A similar k_{OH} value of $3.9 \pm 1.8 \times 10^{-13} \text{ cm}^3$
396 $\text{molec.}^{-1} \text{ s}^{-1}$ was obtained. Despite differences between the SE and Amazon studies, the similarity
397 of results from both studies increases our confidence in the derived value of the heterogeneous
398 reaction rate coefficient.

399 To investigate k_{OH} of OA, multiple experiments (usually with $\text{RH} < 30\%$) with laboratory-
400 generated different types of OA have been conducted. The bulk of those OA in the lab usually
401 had mobility particle sizes ranging from 100-300 nm (Table 1), similar to that of IEPOX-SOA in
402 SE US (wet size=415 nm). The k_{OH} value of IEPOX-SOA determined here is similar to
403 heterogeneous k_{OH} determined in those laboratory studies, including highly-oxidized OA (e.g.
404 citric acid; $3.3 - 7.6 \times 10^{-13} \text{ cm}^3 \text{ molec.}^{-1} \text{ s}^{-1}$) (Kessler et al., 2012), levoglucosan ($1.4 - 4.3 \times 10^{-13}$
405 $\text{cm}^3 \text{ molec.}^{-1} \text{ s}^{-1}$) (Slade and Knopf, 2014), and pure erythritol ($2.5 \times 10^{-13} \text{ cm}^3 \text{ molec.}^{-1} \text{ s}^{-1}$), which
406 has a similar structure to the 2-methyltetrols in IEPOX-SOA (Kessler et al., 2010). A summary
407 of k_{OH} in this study and other laboratory studies with additional experimental information for
408 each study is shown in Table 1.

409 A dependence of k_{OH} on ambient RH was found in both the SE US and Amazon studies,
410 with larger k_{OH} at high RH, especially above 90% RH (Fig. 7). This effect may be due to higher
411 liquid water content, leading to a larger surface area that facilitates faster OH uptake to the
412 aerosol phase and thus resulting in faster k_{OH} values (Slade and Knopf, 2014). Accounting for
413 liquid water content, the calculated particle surface areas show similar trends to k_{OH} , in both
414 studies, as shown in Fig. 7. The values of both parameters increase with RH (especially for
415 $\text{RH} > 90\%$).

416 An alternative explanation for the measured RH dependence would be the influence of
417 diffusion limitations. However, at the RH levels studied here ($>40\%$), diffusion limitations of



418 OH in the aerosol phase are thought to be negligible (calculated lifetime of bulk diffusion of OH
419 radical < 1 s). The diffusion coefficient of OH radical in liquid phase ($>10^{-14}$ m² s⁻¹) was obtained
420 from other laboratory-generated OA (e.g. α -pinene derived SOA, levoglucosan particles)
421 (Renbaum-Wolff et al., 2013; Arangio et al., 2015; Li et al., 2015b). Li et al. (2015b) reported
422 that the diffusion of NH₃ on laboratory biogenic SOA is only slowed at much lower transition
423 RH (10-40%) than that for liquid/solid phase transition (50-80%). This supports that under the
424 conditions in SE and Amazon studies diffusion limitations should not play a role.

425 The ambient lifetime of IEPOX-SOA due to the heterogeneous reaction with OH radicals
426 was estimated to be more than 2 weeks (19 \pm 9 days) based on the average k_{OH} ($4.0\pm 2.0\times 10^{-13}$ cm³
427 molec.⁻¹ s⁻¹), assuming an average ambient OH concentration of 1.5×10^6 molec. cm⁻³. A similar
428 lifetime can be estimated for the Amazon study. Longer lifetimes of 48 days in SE US study and
429 99 days in Amazon study were estimated when the observed average 24h OH concentration in
430 both studies (0.6×10^6 molecule cm⁻³ in SE US and 0.3×10^6 molecule cm⁻³ in Amazon) were used
431 (Krechmer et al., 2015). The long lifetime of IEPOX-SOA against heterogeneous oxidation is
432 consistent with the estimated lifetime of total OA in urban and forested areas (Ortega et al.,
433 2015; Palm et al., 2016), and also pure highly-oxidized OA (1-2 weeks) in laboratory studies
434 (Kessler et al., 2010; Kessler et al., 2012).

435 3.4 Fate of Oxidized IEPOX-SOA mass

436 It is of interest to determine whether the mass of IEPOX-SOA continues to be present in
437 the aerosol after OH heterogeneous oxidation, albeit as a different chemical form, or whether it
438 evaporates from the particles. Functionalization reactions would favor the former, while
439 fragmentation reactions would favor the latter (George et al., 2007).

440 At lower OH exposures ($<1\times 10^{12}$ molec. cm⁻³ s) during daytime, SOA formation (non-
441 IEPOX-SOA) was observed in the OFR (e.g., from monoterpene and sesquiterpenes oxidation,
442 Fig. 6b), making it difficult to discern whether functionalization or fragmentation dominated for
443 IEPOX-SOA losses. However, at OH exposures in the OFR above 1×10^{12} molec. cm⁻³ s, net
444 SOA formation from ambient air was no longer observed. This is presumably due to organic
445 vapors undergoing multiple generations of oxidation and fragmenting in the gas phase in the
446 OFR (Palm et al., 2016). For that OH exposure range, changes of the aerosol phase should be
447 dominated by heterogeneous reactions. In this regime, OA mass was lost at a rapid rate of ~ 6 %
448 OA mass per 1×10^{12} molec. cm⁻³ s of OH exposure through volatilization. A very similar rate



449 was observed for the IEPOX-SOA ($\sim 7\%$ per 1×10^{12} molec. cm^{-3} s), which implies that the main
450 loss mechanism of IEPOX-SOA at higher OH exposures is due to volatilization following
451 fragmentation. In the period when 80-90% of OA was composed of IEPOX-SOA, the OA also
452 showed an up to 70% mass loss (Fig. S20), confirming the conclusion that a high fraction of
453 IEPOX-SOA was volatilized to the gas phase after heterogeneous reaction at higher OH
454 exposures.

455 The aerosol mass losses of IEPOX-SOA and OA into gas phase are consistent with
456 laboratory experiments of heterogeneous reaction of pure erythritol particles (a surrogate of the
457 IEPOX-SOA tracer 2-methyltetrols, see Fig. 6b), which also showed that OH oxidation led to
458 formation of volatile products escaping to the gas phase (Kessler et al., 2010; Kroll et al., 2015).
459 We note however that IEPOX-SOA is mostly composed of oligomers, rather than monomers as
460 with erythritol.

461 3.5 Estimation of reactive uptake coefficient (γ) of OH

462 By quantifying the removal of IEPOX-SOA in the aerosol phase, an effective reactive
463 uptake coefficient of OH (γ_{OH}) on the aerosol in the OFR can be estimated. To our knowledge,
464 this is the first time that γ_{OH} has been derived from measurements of ambient SOA aging.

465 The variable γ_{OH} can be calculated from k_{OH} per Smith et al. (2009):

$$467 \gamma_{\text{OH}} = \frac{4 \cdot k_{\text{OH}} \cdot V_{\text{IEPOX-SOA}} \cdot \rho_0 \cdot N_{\text{A}}}{\bar{c} \cdot S_{\text{IEPOX-SOA}} \cdot MW_{\text{IEPOX-SOA}}} = \frac{4 \cdot k_{\text{OH}} \cdot D_{\text{surf}} \cdot \rho_0 \cdot N_{\text{A}}}{\bar{c} \cdot MW_{\text{IEPOX-SOA}}}, \quad (3)$$

468
469 where k_{OH} is the heterogeneous reaction rate coefficient of IEPOX-SOA discussed above
470 ($4.2 \pm 2.1 \times 10^{-13}$ cm^3 molec. $^{-1}$ s $^{-1}$); ρ_0 is density of aerosol in OFR, which is estimated as 1.46 ± 0.49
471 g cm^{-3} based on the aerosol composition (Fig. S15). N_{A} is Avogadro's number; \bar{c} is the mean
472 speed of gas-phase OH radicals, calculated as $(8RT/\pi M)^{0.5}$ (R is the universal gas constant, T is
473 the temperature in K, and M is the molar mass of the OH radical). The calculated \bar{c} for OH (at
474 293 K) is 604 m s $^{-1}$. $MW_{\text{IEPOX-SOA}}$ is the molar mass of IEPOX-SOA. The estimated
475 $MW_{\text{IEPOX-SOA}} = 270$ g mol $^{-1}$ was used here, which is similar to isoprene-SOA molar mass of 252
476 g mol $^{-1}$ estimated from a separate flow tube study based on CCN measurement (King et al.,
477 2010). An uncertainty of 30% is assigned to $MW_{\text{IEPOX-SOA}}$. $V_{\text{IEPOX-SOA}}$ and $S_{\text{IEPOX-SOA}}$ are the
478 mean volume and surface areas of IEPOX-SOA. If we assume IEPOX-SOA is uniformly mixed
479 with the other aerosol species, and independent of particle size, then IEPOX-SOA will account



480 for $x\%$ of total aerosol volume (V_{total}) and $x\%$ of total aerosol surface area (S_{total}). The ratio
481 between $V_{IEPOX-SOA}$ and $S_{IEPOX-SOA}$ can be expressed as: $x\% \times V_{total} / x\% \times S_{total} = V_{total} / S_{total}$.
482 Values of x varied from 0-90 based on source apportionment results. However, the exact value of
483 x is not needed here since it eventually was canceled out in the calculation. For a spherical
484 particle V_{total} / S_{total} equals to $d_{surf} / 6$. d_{surf} is defined as surface-weighted particle diameter.
485 The dried surface-weighted aerodynamic size distribution of m/z 82 (background corrected),
486 tracer of IEPOX-SOA (Hu et al., 2015), peaks around 400 nm (Fig. 8), which is equivalent to
487 mobility size of ~ 274 nm. By applying the average particle size growth factor of 1.5 calculated
488 from average kappa (0.27) and ambient RH (Nguyen et al., 2014b), the average d_{surf} of wet
489 IEPOX-SOA is estimated as 410 nm; Similar method was applied to calculate d_{surf} of wet
490 IEPOX-SOA in Amazon study, which is finally calculated to be 490 nm.

491 The average mass-weighted aerodynamic size distribution of m/z 82 in SOAS and Amazon
492 ($d_{va} \sim 500$ nm and 600 nm) is consistent with that of sulfate ($d_{va} \sim 450$ nm and 510 nm), which
493 may indicate sulfate control of the IEPOX uptake formation pathway (Xu et al., 2014; Liao et al.,
494 2015; Marais et al., 2016). Both peaks of m/z 82 and sulfate were systematically larger than of
495 total OA ($d_{va} \sim 370$ or 400 nm), suggesting the IEPOX-SOA formation in SE US and Amazon
496 studies may be partially contributed by aqueous/cloud processing (Meng and Seinfeld, 1994).
497 The systematically higher oxidation level of IEPOX-SOA in the ambient air than from chamber
498 studies also support this conclusion (Chen et al., 2015; Hu et al., 2015).

499 Finally, γ_{OH} is estimated as 0.59 ± 0.33 under a range of OH concentrations between 10^7 - 10^{10}
500 molec. cm^{-3} , which is consistent with the range of γ_{OH} (0.37-0.77) calculated for highly oxidized
501 OA in laboratory studies (Table 1). The uncertainty of γ_{OH} was estimated by MonteCarlo
502 simulation, propagated from errors of each parameter in equation (2) (50% for k_{OH} , 30% for d_{surf} ,
503 28% for ρ_0 , and 30% for $MW_{IEPOX-SOA}$). When considering the apparent RH effect on k_{OH} , the
504 estimated γ_{OH} varies between 0.34-1.19. The γ_{OH} above 1 at the highest RH range (90-100%)
505 might be due to secondary reactions of IEPOX-SOA in the more dilute liquid phase. The
506 estimated γ_{OH} in Amazon study is around 0.68 ± 0.38 .

507 Ambient particles in both SOAS and GoAmazon were liquid as quantified by particle
508 bounce experiments (Bateman et al., 2015; Pajunoja et al., 2016) and thus kinetic limitations to
509 OH uptake in the OFR should not play a role (Li et al., 2015). In this study, we calculated γ_{OH}
510 based on a wide range of OH concentrations ($10^7 - 10^{10}$ molec. cm^{-3}). Several laboratory



511 experiments suggest that OH uptake should obey the Langmuir–Hinshelwood (LH) kinetic
512 mechanism, where γ_{OH} tends to lower under higher OH concentrations, because of a saturation of
513 surface reactive sites at higher OH concentrations (Che et al., 2009; George and Abbatt, 2010;
514 Slade and Knopf, 2013). We have calculated k_{OH} at different OH exposure ranges (10^{10} to 10^{11} -
515 10^{13} molec. $\text{cm}^{-3} \text{s}^{-1}$, Fig. S22). No obvious OH dependence of k_{OH} (γ_{OH}) was found above 3×10^9
516 molec. cm^{-3} (beyond where k_{OH} calculation is more robust), which suggests the γ_{OH} calculated in
517 this study does not depend on OH concentration. It may be because in this study the OH uptake
518 happened in the liquid particle, causing OH diffusion not to be limited by surface dynamics.
519 More consideration of other factors (e.g., surface regeneration due to volatilization; aerosol
520 phase influence) should be explored in future studies of the γ_{OH} for IEPOX-SOA.

521 4. Conclusions

522 We investigated volatility and aging process of IEPOX-SOA during the late spring and
523 early summer of SE US and the dry season of central Amazonia with field-deployed
524 thermodenuder and oxidation flow reactor. IEPOX-SOA had a volatility distribution much lower
525 than those of the monomer tracers that have been reported as comprising most of its mass. Much
526 of IEPOX-SOA likely exists as oligomers in the aerosol phase. The kinetics of decomposition of
527 oligomers to monomers needs further investigation to fully constrain the lifetime of IEPOX-SOA
528 against evaporation.

529 The formation of IEPOX-SOA in the field and in the OFR flow reactor was investigated. In
530 contrast to the efficient IEPOX uptake in the ambient air, negligible IEPOX-SOA was formed in
531 the OFR under OH oxidation, as the OFR as used here cannot accelerate processes such as
532 aerosol uptake and reactions that do not scale with OH. Simulation results indicate that adding
533 $\sim 100 \mu\text{g m}^{-3}$ of pure H_2SO_4 to the ambient air would allow to efficiently form IEPOX-SOA in the
534 reactor. Photolysis and evaporation of IEPOX-SOA in the OFR contributed negligibly to
535 IEPOX-SOA loss. From the OFR results, we determined the lifetime of IEPOX-SOA through
536 heterogeneous reaction with OH radicals ($k_{\text{OH}} = 4.0 \pm 2.0 \times 10^{-13} \text{ cm}^3 \text{ molecule}^{-1} \text{ s}^{-1}$ in SE US and
537 $3.9 \pm 1.8 \times 10^{-13} \text{ cm}^3 \text{ molecule}^{-1} \text{ s}^{-1}$ in the Amazon) is equivalent to more than a 2-week
538 photochemical aging lifetime (assuming $\text{OH} = 1.5 \times 10^6 \text{ molec. cm}^{-3}$). The mass lost at high OH
539 exposures is mainly volatilized, rather than transformed into other aerosol species with different
540 composition, which suggests fragmentation plays an important role during ambient aging
541 process.



542 Values of effective γ_{OH} based on the measured IEPOX-SOA k_{OH} and other particle
543 parameters were determined to be 0.59 ± 0.33 in SE US and 0.68 ± 0.38 in Amazon with no
544 dependence on OH concentration over the range 10^7 - 10^{10} molecule cm^{-3} . This is the first time of
545 γ_{OH} was estimated based on ambient SOA. Positive correlation between γ_{OH} and wet particle
546 surface areas (RH dependent) suggest that OH uptake is surface area-limited. The substantially
547 larger size distribution of IEPOX-SOA tracer m/z 82 and sulfate vs. bulk OA suggests that
548 IEPOX-SOA formation in SE US study may be controlled by sulfate and/or influenced by cloud
549 processing. However, the effect of aqueous processing under very dilute conditions relevant to
550 clouds has not been investigated to our knowledge. Our results provide constraints on the sinks
551 of IEPOX-SOA, which are useful to better quantify OA impacts on air quality and climate.
552

553 Acknowledgements

554 This study was partially supported by EPRI-10004734, NSF AGS-1243354 and AGS-1360834,
555 NASA NNX15AT96G, DOE (BER/ASR) DE-SC0011105, and NOAA NA13OAR4310063.
556 BBP and JEK were partially supported by EPA STAR Fellowships (FP-91761701-0 & FP-
557 91770901-0). We thank Annmarie Carlton, Eric Edgerton, and Karsten Baumann for their
558 organization of the SOAS Supersite; Cassandra Gaston and Joel Thornton from the University of
559 Washington for advice in the use of their IEPOX uptake model; Jian Wang from Brookhaven
560 National Laboratory for advice on aerosol hygroscopicity during GoAmazon2014/5; Ying-Hsuan
561 Lin and Jason D. Surratt from the University of North Carolina for sharing their published MAC
562 data of IEPOX-SOA; Hongyu Guo and Rodney J. Weber from Georgia Institute of Technology
563 for providing their estimated pH for comparison to our pH calculation results; and John Crouse
564 and Paul Wennberg from Caltech for gas-phase IEPOX and ISOPOOH data in SOAS. This paper
565 has not been reviewed by EPA and no endorsement should be inferred. (A portion of) The
566 research was performed using EMSL, a DOE Office of Science User Facility sponsored by the
567 Office of Biological and Environmental Research and located at Pacific Northwest National
568 Laboratory. SEARCH network operations are supported by Southern Company and EPRI.

569

570

571

572 **References**

- 573 Arangio, A. M., Slade, J. H., Berkemeier, T., Pöschl, U., Knopf, D. A., and Shiraiwa, M.: Multiphase
574 Chemical Kinetics of OH Radical Uptake by Molecular Organic Markers of Biomass Burning
575 Aerosols: Humidity and Temperature Dependence, Surface Reaction, and Bulk Diffusion, *J. Phys.*
576 *Chem. A*, 10.1021/jp510489z, 2015.
- 577 Bateman, A. P., Gong, Z., Liu, P., Sato, B., Cirino, G., Zhang, Y., Artaxo, P., Bertram, A. K., Manzi, A. O.,
578 Rizzo, L. V., Souza, R. A. F., Zaveri, R. A., and Martin, S. T.: Sub-micrometre particulate matter is
579 primarily in liquid form over Amazon rainforest, *Nature Geosci.*, advance online publication,
580 10.1038/ngeo2599, 2015.
- 581 Bates, K. H., Crounse, J. D., St. Clair, J. M., Bennett, N. B., Nguyen, T. B., Seinfeld, J. H., Stoltz, B. M., and
582 Wennberg, P. O.: Gas Phase Production and Loss of Isoprene Epoxydiols, *J. Phys. Chem. A*, 118,
583 1237-1246, 10.1021/jp4107958, 2014.
- 584 Bates, K. H., Nguyen, T. B., Teng, A. P., Crounse, J. D., Kjaergaard, H. G., Stoltz, B. M., Seinfeld, J. H., and
585 Wennberg, P. O.: Production and Fate of C4 Dihydroxycarbonyl Compounds from Isoprene
586 Oxidation, *J. Phys. Chem. A*, 120, 106-117, 10.1021/acs.jpca.5b10335, 2015.
- 587 Budisulistiorini, S. H., Canagaratna, M. R., Croteau, P. L., Marth, W. J., Baumann, K., Edgerton, E. S.,
588 Shaw, S. L., Knipping, E. M., Worsnop, D. R., Jayne, J. T., Gold, A., and Surratt, J. D.: Real-Time
589 Continuous Characterization of Secondary Organic Aerosol Derived from Isoprene Epoxydiols in
590 Downtown Atlanta, Georgia, Using the Aerodyne Aerosol Chemical Speciation Monitor, *Environ.*
591 *Sci. Technol.*, 47, 5686-5694, 10.1021/es400023n, 2013.
- 592 Budisulistiorini, S. H., Li, X., Bairai, S. T., Renfro, J., Liu, Y., Liu, Y. J., McKinney, K. A., Martin, S. T., McNeill,
593 V. F., Pye, H. O. T., Nenes, A., Neff, M. E., Stone, E. A., Mueller, S., Knote, C., Shaw, S. L., Zhang,
594 Z., Gold, A., and Surratt, J. D.: Examining the effects of anthropogenic emissions on isoprene-
595 derived secondary organic aerosol formation during the 2013 Southern Oxidant and Aerosol
596 Study (SOAS) at the Look Rock, Tennessee ground site, *Atmos. Chem. Phys.*, 15, 8871-8888,
597 10.5194/acp-15-8871-2015, 2015.
- 598 Canonaco, F., Crippa, M., Slowik, J. G., Baltensperger, U., and Prévôt, A. S. H.: SoFi, an IGOR-based
599 interface for the efficient use of the generalized multilinear engine (ME-2) for the source
600 apportionment: ME-2 application to aerosol mass spectrometer data, *Atmos. Meas. Tech.*, 6,
601 3649-3661, 10.5194/amt-6-3649-2013, 2013.
- 602 Cappa, C. D., and Jimenez, J. L.: Quantitative estimates of the volatility of ambient organic aerosol,
603 *Atmos. Chem. Phys.*, 10, 5409-5424, 10.5194/acp-10-5409-2010, 2010.
- 604 Chattopadhyay, S., and Ziemann, P. J.: Vapor Pressures of Substituted and Unsubstituted
605 Monocarboxylic and Dicarboxylic Acids Measured Using an Improved Thermal Desorption
606 Particle Beam Mass Spectrometry Method, *Aerosol. Sci. Tech.*, 39, 1085-1100,
607 10.1080/02786820500421547, 2005.
- 608 Che, D. L., Smith, J. D., Leone, S. R., Ahmed, M., and Wilson, K. R.: Quantifying the reactive uptake of OH
609 by organic aerosols in a continuous flow stirred tank reactor, *Phys. Chem. Chem. Phys.* 11, 7885-
610 7895, 10.1039/b904418c, 2009.
- 611 Chen, Q., Farmer, D. K., Rizzo, L. V., Pauliquevis, T., Kuwata, M., Karl, T. G., Guenther, A., Allan, J. D., Coe,
612 H., Andreae, M. O., Pöschl, U., Jimenez, J. L., Artaxo, P., and Martin, S. T.: Submicron particle
613 mass concentrations and sources in the Amazonian wet season (AMAZE-08), *Atmos. Chem.*
614 *Phys.*, 15, 3687-3701, 10.5194/acp-15-3687-2015, 2015.
- 615 DeCarlo, P. F., Kimmel, J. R., Trimborn, A., Northway, M. J., Jayne, J. T., Aiken, A. C., Gonin, M., Fuhrer, K.,
616 Horvath, T., Docherty, K. S., Worsnop, D. R., and Jimenez, J. L.: Field-deployable, high-resolution,
617 time-of-flight aerosol mass spectrometer, *Anal. Chem.*, 78, 8281-8289, Doi 10.1021/Ac061249n,
618 2006.



- 619 Dzepina, K., Jimenez, J. L., Cappa, C. D., Volkamer, R. M., Madronich, S., DeCarlo, P. F., and Zaveri, R. A.:
620 Modeling the Multiday Evolution and Aging of Secondary Organic Aerosol During MILAGRO
621 2006, *Environ. Sci. Technol.*, 45, 3496-3503, 10.1021/es103186f, 2011.
- 622 Eddingsaas, N. C., VanderVelde, D. G., and Wennberg, P. O.: Kinetics and Products of the Acid-Catalyzed
623 Ring-Opening of Atmospherically Relevant Butyl Epoxy Alcohols, *J. Phys. Chem. A*, 114, 8106-
624 8113, 10.1021/jp103907c, 2010.
- 625 Faulhaber, A. E., Thomas, B. M., Jimenez, J. L., Jayne, J. T., Worsnop, D. R., and Ziemann, P. J.:
626 Characterization of a thermodenuder-particle beam mass spectrometer system for the study of
627 organic aerosol volatility and composition, *Atmos. Meas. Tech.*, 2, 15-31, 10.5194/amt-2-15-
628 2009, 2009.
- 629 Fleming, G., Anderson, M. M., Harrison, A. J., and Pickett, L. W.: Effect of Ring Size on the Far Ultraviolet
630 Absorption and Photolysis of Cyclic Ethers, *J. Phys. Chem. A*, 30, 351-354, 10.1063/1.1729951,
631 1959.
- 632 Froyd, K. D., Murphy, S. M., Murphy, D. M., de Gouw, J. A., Eddingsaas, N. C., and Wennberg, P. O.:
633 Contribution of isoprene-derived organosulfates to free tropospheric aerosol mass, *Proc. Natl.*
634 *Acad. Sci. USA*, 107 21360–21365, doi: 10.1073/pnas.1012561107, 2010.
- 635 Gaston, C. J., Riedel, T. P., Zhang, Z., Gold, A., Surratt, J. D., and Thornton, J. A.: Reactive Uptake of an
636 Isoprene-Derived Epoxydiol to Submicron Aerosol Particles, *Environ. Sci. Technol.*, 48,
637 11178–11186, 10.1021/es5034266, 2014.
- 638 George, C., Ammann, M., D'Anna, B., Donaldson, D. J., and Nizkorodov, S. A.: Heterogeneous
639 Photochemistry in the Atmosphere, *Chem. Rev.*, 10.1021/cr500648z, 2015.
- 640 George, I., Vlasenko, A., Slowik, J., and Abbatt, J.: Heterogeneous Oxidation of Saturated Organic
641 Particles by OH, in: *Nucleation and Atmospheric Aerosols*, edited by: O'Dowd, C., and Wagner,
642 P., Springer Netherlands, 736-740, 2007.
- 643 George, I. J., and Abbatt, J. P. D.: Heterogeneous oxidation of atmospheric aerosol particles by gas-phase
644 radicals, *Nat. Chem.*, 2, 713-722, 2010.
- 645 Guenther, A. B., Jiang, X., Heald, C. L., Sakulyanontvittaya, T., Duhl, T., Emmons, L. K., and Wang, X.: The
646 Model of Emissions of Gases and Aerosols from Nature version 2.1 (MEGAN2.1): an extended
647 and updated framework for modeling biogenic emissions, *Geosci. Model Dev.*, 5, 1471-1492,
648 10.5194/gmd-5-1471-2012, 2012.
- 649 Hallquist, M., Wenger, J. C., Baltensperger, U., Rudich, Y., Simpson, D., Claeys, M., Dommen, J., Donahue,
650 N. M., George, C., Goldstein, A. H., Hamilton, J. F., Herrmann, H., Hoffmann, T., Iinuma, Y., Jang,
651 M., Jenkin, M. E., Jimenez, J. L., Kiendler-Scharr, A., Maenhaut, W., McFiggans, G., Mentel, T. F.,
652 Monod, A., Prevot, A. S. H., Seinfeld, J. H., Surratt, J. D., Szmigielski, R., and Wildt, J.: The
653 formation, properties and impact of secondary organic aerosol: current and emerging issues,
654 *Atmos. Chem. Phys.*, 9, 5155-5236, 2009.
- 655 Hansen, D. A., Edgerton, E. S., Hartsell, B. E., Jansen, J. J., Kandasamy, N., Hidy, G. M., and Blanchard, C.
656 L.: The Southeastern Aerosol Research and Characterization Study: Part 1—Overview, *J. Air
657 Waste Manage*, 53, 1460-1471, 10.1080/10473289.2003.10466318, 2003.
- 658 Hu, W. W., Campuzano-Jost, P., Palm, B. B., Day, D. A., Ortega, A. M., Hayes, P. L., Krechmer, J. E., Chen,
659 Q., Kuwata, M., Liu, Y. J., de Sá, S. S., McKinney, K., Martin, S. T., Hu, M., Budisulistiorini, S. H.,
660 Riva, M., Surratt, J. D., St. Clair, J. M., Isaacman-Van Wertz, G., Yee, L. D., Goldstein, A. H.,
661 Carbone, S., Brito, J., Artaxo, P., de Gouw, J. A., Koss, A., Wisthaler, A., Mikoviny, T., Karl, T.,
662 Kaser, L., Jud, W., Hansel, A., Docherty, K. S., Alexander, M. L., Robinson, N. H., Coe, H., Allan, J.
663 D., Canagaratna, M. R., Paulot, F., and Jimenez, J. L.: Characterization of a real-time tracer for
664 isoprene epoxydiols-derived secondary organic aerosol (IEPOX-SOA) from aerosol mass
665 spectrometer measurements, *Atmos. Chem. Phys.*, 15, 11807-11833, 10.5194/acp-15-11807-
666 2015, 2015.



- 667 Huffman, J. A., Docherty, K. S., Aiken, A. C., Cubison, M. J., Ulbrich, I. M., DeCarlo, P. F., Sueper, D., Jayne,
668 J. T., Worsnop, D. R., Ziemann, P. J., and Jimenez, J. L.: Chemically-resolved aerosol volatility
669 measurements from two megacity field studies, *Atmos. Chem. Phys.*, 9, 7161-7182, 2009a.
- 670 Huffman, J. A., Ziemann, P. J., Jayne, J. T., Worsnop, D. R., and Jimenez, J. L.: Development and
671 Characterization of a Fast-Stepping/Scanning Thermodenuder for Chemically-Resolved Aerosol
672 Volatility Measurements (vol 42, pg 395, 2008), *Aerosol Sci. Tech.*, 43, 273-273, Doi
673 10.1080/02786820802616885, 2009b.
- 674 Isaacman-VanWertz, G., Goldstein, A. H., Yee, L. D., Kreisberg, N. M., Wernis, R., Moss, J. A., Hering, S. V.,
675 de sa, S. S., Martin, S. T., Alexander, M. L., Palm, B. B., Hu, W. W., Campuzano-Jost, P., Day, D. A.,
676 Jimenez, J. L., Riva, M., Surratt, J. D., Edgerton, E., Baumann, K., Viegas, J., Manzi, A., Souza, R.,
677 and Artaxo, P.: Observations of gas-particle partitioning of biogenic oxidation products in
678 forested environments, *Environ. Sci. Technol.*, Submitted, 2016.
- 679 Isaacman, G., Chan, A. W. H., Nah, T., Worton, D. R., Ruehl, C. R., Wilson, K. R., and Goldstein, A. H.:
680 Heterogeneous OH Oxidation of Motor Oil Particles Causes Selective Depletion of Branched and
681 Less Cyclic Hydrocarbons, *Environ. Sci. Technol.*, 46, 10632-10640, 10.1021/es302768a, 2012.
- 682 Kanakidou, M., Seinfeld, J. H., Pandis, S. N., Barnes, I., Dentener, F. J., Facchini, M. C., Van Dingenen, R.,
683 Ervens, B., Nenes, A., Nielsen, C. J., Swietlicki, E., Putaud, J. P., Balkanski, Y., Fuzzi, S., Horth, J.,
684 Moortgat, G. K., Winterhalter, R., Myhre, C. E. L., Tsigaridis, K., Vignati, E., Stephanou, E. G., and
685 Wilson, J.: Organic aerosol and global climate modelling: a review, *Atmos. Chem. Phys.*, 5, 1053-
686 1123, 2005.
- 687 Kang, E., Root, M. J., Toohey, D. W., and Brune, W. H.: Introducing the concept of Potential Aerosol Mass
688 (PAM), *Atmos. Chem. Phys.*, 7, 5727-5744, 10.5194/acp-7-5727-2007, 2007.
- 689 Karl, T., Guenther, A., Yokelson, R. J., Greenberg, J., Potosnak, M., Blake, D. R., and Artaxo, P.: The
690 tropical forest and fire emissions experiment: Emission, chemistry, and transport of biogenic
691 volatile organic compounds in the lower atmosphere over Amazonia, *J. Geophys. Res.*, 112,
692 10.1029/2007jd008539, 2007.
- 693 Kessler, S. H., Smith, J. D., Che, D. L., Worsnop, D. R., Wilson, K. R., and Kroll, J. H.: Chemical Sinks of
694 Organic Aerosol: Kinetics and Products of the Heterogeneous Oxidation of Erythritol and
695 Levoglucosan, *Environ. Sci. Technol.*, 44, 7005-7010, Doi 10.1021/Es101465m, 2010.
- 696 Kessler, S. H., Nah, T., Daumit, K. E., Smith, J. D., Leone, S. R., Kolb, C. E., Worsnop, D. R., Wilson, K. R.,
697 and Kroll, J. H.: OH-Initiated Heterogeneous Aging of Highly Oxidized Organic Aerosol, *J. Phys.*
698 *Chem. A*, 116, 6358-6365, 10.1021/jp212131m, 2012.
- 699 King, S. M., Rosenoern, T., Shilling, J. E., Chen, Q., Wang, Z., Biskos, G., McKinney, K. A., Pöschl, U., and
700 Martin, S. T.: Cloud droplet activation of mixed organic-sulfate particles produced by the
701 photooxidation of isoprene, *Atmos. Chem. Phys.*, 10, 3953-3964, 10.5194/acp-10-3953-2010,
702 2010.
- 703 Krechmer, J. E., Coggon, M. M., Massoli, P., Nguyen, T. B., Crouse, J. D., Hu, W., Day, D. A., Tyndall, G.
704 S., Henze, D. K., Rivera-Rios, J. C., Nowak, J. B., Kimmel, J. R., Mauldin, R. L., Stark, H., Jayne, J. T.,
705 Sipilä, M., Junninen, H., St. Clair, J. M., Zhang, X., Feiner, P. A., Zhang, L., Miller, D. O., Brune, W.
706 H., Keutsch, F. N., Wennberg, P. O., Seinfeld, J. H., Worsnop, D. R., Jimenez, J. L., and
707 Canagaratna, M. R.: Formation of Low Volatility Organic Compounds and Secondary Organic
708 Aerosol from Isoprene Hydroxyhydroperoxide Low-NO Oxidation, *Environ. Sci. Technol.*, 49
709 10330-10339, 10.1021/acs.est.5b02031, 2015.
- 710 Kroll, J. H., Lim, C. Y., Kessler, S. H., and Wilson, K. R.: Heterogeneous Oxidation of Atmospheric Organic
711 Aerosol: Kinetics of Changes to the Amount and Oxidation State of Particle-Phase Organic
712 Carbon, *J. Phys. Chem. A*, 10.1021/acs.jpca.5b06946, 2015.
- 713 Lambe, A. T., Ahern, A. T., Williams, L. R., Slowik, J. G., Wong, J. P. S., Abbatt, J. P. D., Brune, W. H., Ng, N.
714 L., Wright, J. P., Croasdale, D. R., Worsnop, D. R., Davidovits, P., and Onasch, T. B.:



- 715 Characterization of aerosol photooxidation flow reactors: heterogeneous oxidation, secondary
716 organic aerosol formation and cloud condensation nuclei activity measurements, *Atmos. Meas.*
717 *Tech.*, 4, 445-461, 10.5194/amt-4-445-2011, 2011.
- 718 Li, R., Palm, B. B., Ortega, A. M., Hlywiak, J. A., Hu, W., Peng, Z., Day, D. A., Knote, C., Brune, W. H., de
719 Gouw, J. A., and Jimenez, J. L.: Modeling the Radical Chemistry in an Oxidation Flow Reactor:
720 Radical Formation and Recycling, Sensitivities, and OH Exposure Estimation Equation, *J. Phys.*
721 *Chem. A*, 10.1021/jp509534k, 2015a.
- 722 Li, Y. J., Liu, P., Gong, Z., Wang, Y., Bateman, A. P., Bergoend, C., Bertram, A. K., and Martin, S. T.:
723 Chemical Reactivity and Liquid/Nonliquid States of Secondary Organic Material, *Environ. Sci.*
724 *Technol.*, 10.1021/acs.est.5b03392, 2015b.
- 725 Liao, J., Froyd, K. D., Murphy, D. M., Keutsch, F. N., Yu, G., Wennberg, P. O., St. Clair, J. M., Crouse, J. D.,
726 Wisthaler, A., Mikoviny, T., Jimenez, J. L., Campuzano Jost, P., Day, D. A., Hu, W., Ryerson, T. B.,
727 Pollack, I. B., Peischl, J., Anderson, B. E., Ziemba, L. D., Blake, D. R., Meinardi, S., and Diskin, G.:
728 Airborne measurements of organosulfates over the continental US, *J. Geophys. Res.*, 120, 2990-
729 3005, 10.1002/2014jd022378, 2015.
- 730 Lin, Y.-H., Zhang, Z., Docherty, K. S., Zhang, H., Budisulistiorini, S. H., Rubitschun, C. L., Shaw, S. L.,
731 Knipping, E. M., Edgerton, E. S., Kleindienst, T. E., Gold, A., and Surratt, J. D.: Isoprene Epoxydiols
732 as Precursors to Secondary Organic Aerosol Formation: Acid-Catalyzed Reactive Uptake Studies
733 with Authentic Compounds, *Environ. Sci. Technol.*, 46, 250-258, 10.1021/es202554c, 2012.
- 734 Lin, Y.-H., Budisulistiorini, S. H., Chu, K., Siejack, R. A., Zhang, H., Riva, M., Zhang, Z., Gold, A., Kautzman,
735 K. E., and Surratt, J. D.: Light-Absorbing Oligomer Formation in Secondary Organic Aerosol from
736 Reactive Uptake of Isoprene Epoxydiols, *Environ. Sci. Technol.*, 48, 12012-12021,
737 10.1021/es503142b, 2014.
- 738 Liu, Y., Ivanov, A. V., Zelenov, V. V., and Molina, M. J.: Temperature dependence of OH uptake by
739 carbonaceous surfaces of atmospheric importance, *Russ. J. Phys. Chem. B*, 6, 327-332,
740 10.1134/s199079311202008x, 2012.
- 741 Lopez-Hilfiker, F., Mohr, C., D'Ambro, E. L., Lutz, A., Riedel, T. P., Gaston, C. J., Iyer, S., Zhang, Z., Gold, A.,
742 Surratt, J. D., Lee, B. H., Kurtén, T., Hu, W., Jimenez, J. L., Hallquist, M., and Thornton, J. A.:
743 Molecular composition and volatility of organic aerosol in the Southeastern U.S.: implications for
744 IEPOX derived SOA, *Environ. Sci. Technol.*, 50, pp2200-2209, 10.1021/acs.est.5b04769, 2016.
- 745 Mao, J., Ren, X., Brune, W. H., Olson, J. R., Crawford, J. H., Fried, A., Huey, L. G., Cohen, R. C., Heikes, B.,
746 Singh, H. B., Blake, D. R., Sachse, G. W., Diskin, G. S., Hall, S. R., and Shetter, R. E.: Airborne
747 measurement of OH reactivity during INTEX-B, *Atmos. Chem. Phys.*, 9, 163-173, 10.5194/acp-9-
748 163-2009, 2009.
- 749 Marais, E. A., Jacob, D. J., Jimenez, J. L., Campuzano-Jost, P., Day, D. A., Hu, W., Krechmer, J., Zhu, L.,
750 Kim, P. S., Miller, C. C., Fisher, J. A., Travis, K., Yu, K., Hanisco, T. F., Wolfe, G. M., Arkinson, H. L.,
751 Pye, H. O. T., Froyd, K. D., Liao, J., and McNeill, V. F.: Aqueous-phase mechanism for secondary
752 organic aerosol formation from isoprene: application to the southeast United States and co-
753 benefit of SO₂ emission controls, *Atmos. Chem. Phys.*, 16, 1603-1618, 10.5194/acp-16-1603-
754 2016, 2016.
- 755 Martin, S. T., Andreae, M. O., Althausen, D., Artaxo, P., Baars, H., Borrmann, S., Chen, Q., Farmer, D. K.,
756 Guenther, A., Gunthe, S. S., Jimenez, J. L., Karl, T., Longo, K., Manzi, A., Müller, T., Pauliquevis, T.,
757 Petters, M. D., Prenni, A. J., Pöschl, U., Rizzo, L. V., Schneider, J., Smith, J. N., Swietlicki, E., Tota,
758 J., Wang, J., Wiedensohler, A., and Zorn, S. R.: An overview of the Amazonian Aerosol
759 Characterization Experiment 2008 (AMAZE-08), *Atmos. Chem. Phys.*, 10, 11415-11438,
760 10.5194/acp-10-11415-2010, 2010.
- 761 Martin, S. T., Artaxo, P., Machado, L. A. T., Manzi, A. O., Souza, R. A. F., Schumacher, C., Wang, J.,
762 Andreae, M. O., Barbosa, H. M. J., Fan, J., Fisch, G., Goldstein, A. H., Guenther, A., Jimenez, J. L.,



- 763 Pöschl, U., Silva Dias, M. A., Smith, J. N., and Wendisch, M.: Introduction: Observations and
764 Modeling of the Green Ocean Amazon (GoAmazon2014/5), Atmos. Chem. Phys. Discuss., 15,
765 30175-30210, 10.5194/acpd-15-30175-2015, 2015.
- 766 May, A. A., Levin, E. J. T., Hennigan, C. J., Riipinen, I., Lee, T., Collett, J. L., Jimenez, J. L., Kreidenweis, S.
767 M., and Robinson, A. L.: Gas-particle partitioning of primary organic aerosol emissions: 3.
768 Biomass burning, J. Geophys. Res., 118, 11,327-311,338, 10.1002/jgrd.50828, 2013.
- 769 McNeill, V. F., Yatavelli, R. L. N., Thornton, J. A., Stipe, C. B., and Landgrebe, O.: Heterogeneous OH
770 oxidation of palmitic acid in single component and internally mixed aerosol particles:
771 vaporization and the role of particle phase, Atmos. Chem. Phys., 8, 5465-5476, 10.5194/acp-8-
772 5465-2008, 2008.
- 773 Meng, Z., and Seinfeld, J. H.: On the Source of the Submicrometer Droplet Mode of Urban and Regional
774 Aerosols, Aerosol. Sci. Tech., 20, 253-265, 10.1080/02786829408959681, 1994.
- 775 Nguyen, T. B., Coggon, M. M., Bates, K. H., Zhang, X., Schwantes, R. H., Schilling, K. A., Loza, C. L., Flagan,
776 R. C., Wennberg, P. O., and Seinfeld, J. H.: Organic aerosol formation from the reactive uptake of
777 isoprene epoxydiols (IEPOX) onto non-acidified inorganic seeds, Atmos. Chem. Phys., 14, 3497-
778 3510, 10.5194/acp-14-3497-2014, 2014a.
- 779 Nguyen, T. B., Crouse, J. D., Teng, A. P., St. Clair, J. M., Paulot, F., Wolfe, G. M., and Wennberg, P. O.:
780 Rapid deposition of oxidized biogenic compounds to a temperate forest, Proc. Natl. Acad. Sci.
781 USA, 112, E392-E401, 10.1073/pnas.1418702112, 2015.
- 782 Nguyen, T. K. V., Petters, M. D., Suda, S. R., Guo, H., Weber, R. J., and Carlton, A. G.: Trends in particle-
783 phase liquid water during the Southern Oxidant and Aerosol Study, Atmos. Chem. Phys., 14,
784 10911-10930, 10.5194/acp-14-10911-2014, 2014b.
- 785 Ortega, A. M., Hayes, P. L., Peng, Z., Palm, B. B., Hu, W., Day, D. A., Li, R., Cubison, M. J., Brune, W. H.,
786 Graus, M., Warneke, C., Gilman, J. B., Kuster, W. C., de Gouw, J. A., and Jimenez, J. L.: Real-time
787 measurements of secondary organic aerosol formation and aging from ambient air in an
788 oxidation flow reactor in the Los Angeles area, Atmos. Chem. Phys. Discuss., 15, 21907-21958,
789 10.5194/acpd-15-21907-2015, 2015.
- 790 Paatero, P.: User's guide for positive matrix factorization programs PMF2.EXE and PMF3.EXE, University
791 of Helsinki, Finland, 2007.
- 792 Pajunoja, A., Hu, W., Leong, Y. J., Taylor, N. F., Miettinen, P., Palm, B. B., Mikkonen, S., Collins, D. R.,
793 Jimenez, J. L., and Virtanen, A.: Phase state of ambient aerosol linked with water uptake and
794 chemical aging in the Southeastern US, Atmos. Chem. Phys. Discuss., 2016, 1-25, 10.5194/acp-
795 2016-375, 2016.
- 796 Palm, B. B., Campuzano-Jost, P., Ortega, A. M., Day, D. A., Kaser, L., Jud, W., Karl, T., Hansel, A., Hunter, J.
797 F., Cross, E. S., Kroll, J. H., Peng, Z., Brune, W. H., and Jimenez, J. L.: In situ secondary organic
798 aerosol formation from ambient pine forest air using an oxidation flow reactor, Atmos. Chem.
799 Phys., 16, 2943-2970, 10.5194/acp-16-2943-2016, 2016.
- 800 Pankow, J. F., and Asher, W. E.: SIMPOL.1: a simple group contribution method for predicting vapor
801 pressures and enthalpies of vaporization of multifunctional organic compounds, Atmos. Chem.
802 Phys., 8, 2773-2796, 10.5194/acp-8-2773-2008, 2008.
- 803 Park, J.-H., Ivanov, A. V., and Molina, M. J.: Effect of Relative Humidity on OH Uptake by Surfaces of
804 Atmospheric Importance, J. Phys. Chem. A, 112, 6968-6977, 10.1021/jp8012317, 2008.
- 805 Paulot, F., Crouse, J. D., Kjaergaard, H. G., Kürten, A., St. Clair, J. M., Seinfeld, J. H., and Wennberg, P.
806 O.: Unexpected Epoxide Formation in the Gas-Phase Photooxidation of Isoprene, Science, 325,
807 730-733, 10.1126/science.1172910, 2009.
- 808 Peng, Z., Day, D. A., Ortega, A. M., Palm, B. B., Hu, W. W., Stark, H., Li, R., Tsigaridis, K., Brune, W. H., and
809 Jimenez, J. L.: Non-OH chemistry in oxidation flow reactors for the study of atmospheric



- 810 chemistry systematically examined by modeling, Atmos. Chem. Phys. Discuss., 15, 23543-23586,
811 10.5194/acpd-15-23543-2015, 2015a.
- 812 Peng, Z., Day, D. A., Stark, H., Li, R., Lee-Taylor, J., Palm, B. B., Brune, W. H., and Jimenez, J. L.: HOx
813 radical chemistry in oxidation flow reactors with low-pressure mercury lamps systematically
814 examined by modeling, Atmos. Meas. Tech., 8, 4863-4890, 10.5194/amt-8-4863-2015, 2015b.
- 815 Phillips, S. M., and Smith, G. D.: Light Absorption by Charge Transfer Complexes in Brown Carbon
816 Aerosols, Environ. Sci. Technol. Lett., 1, 382-386, 10.1021/ez500263j, 2014.
- 817 Phillips, S. M., and Smith, G. D.: Further Evidence for Charge Transfer Complexes in Brown Carbon
818 Aerosols from Excitation–Emission Matrix Fluorescence Spectroscopy, J. Phys. Chem. A, 119,
819 4545-4551, 10.1021/jp510709e, 2015.
- 820 Ranjan, M., Presto, A. A., May, A. A., and Robinson, A. L.: Temperature Dependence of Gas–Particle
821 Partitioning of Primary Organic Aerosol Emissions from a Small Diesel Engine, Aerosol. Sci. Tech.,
822 46, 13-21, 10.1080/02786826.2011.602761, 2012.
- 823 Renbaum-Wolff, L., Grayson, J. W., Bateman, A. P., Kuwata, M., Sellier, M., Murray, B. J., Shilling, J. E.,
824 Martin, S. T., and Bertram, A. K.: Viscosity of α -pinene secondary organic material and
825 implications for particle growth and reactivity, Proc. Natl. Acad. Sci. USA, 110, 8014-8019,
826 10.1073/pnas.1219548110, 2013.
- 827 Riedel, T. P., Lin, Y.-H., Budisulistiorini, S. H., Gaston, C. J., Thornton, J. A., Zhang, Z., Vizuete, W., Gold,
828 A., and Surratt, J. D.: Heterogeneous Reactions of Isoprene-Derived Epoxides: Reaction
829 Probabilities and Molar Secondary Organic Aerosol Yield, Environ. Sci. Technol. Lett., 2, 38-42,
830 10.1021/ez500406f, 2015.
- 831 Robinson, N. H., Hamilton, J. F., Allan, J. D., Langford, B., Oram, D. E., Chen, Q., Docherty, K., Farmer, D.
832 K., Jimenez, J. L., Ward, M. W., Hewitt, C. N., Barley, M. H., Jenkin, M. E., Rickard, A. R., Martin, S.
833 T., McFiggans, G., and Coe, H.: Evidence for a significant proportion of Secondary Organic
834 Aerosol from isoprene above a maritime tropical forest, Atmos. Chem. Phys., 11, 1039-1050,
835 10.5194/acp-11-1039-2011, 2011.
- 836 Sharpless, C. M., and Blough, N. V.: The importance of charge-transfer interactions in determining
837 chromophoric dissolved organic matter (CDOM) optical and photochemical properties, Environ.
838 Sci.: Process. & Impacts, 16, 654-671, 10.1039/c3em00573a, 2014.
- 839 Slade, J. H., and Knopf, D. A.: Heterogeneous OH oxidation of biomass burning organic aerosol surrogate
840 compounds: assessment of volatilisation products and the role of OH concentration on the
841 reactive uptake kinetics, Phys. Chem. Chem. Phys., 15, 5898-5915, 10.1039/c3cp44695f, 2013.
- 842 Slade, J. H., and Knopf, D. A.: Multiphase OH oxidation kinetics of organic aerosol: The role of particle
843 phase state and relative humidity, Geophys. Res. Lett., 41, 5297-5306, 10.1002/2014gl060582,
844 2014.
- 845 Slowik, J. G., Wong, J. P. S., and Abbatt, J. P. D.: Real-time, controlled OH-initiated oxidation of biogenic
846 secondary organic aerosol, Atmos. Chem. Phys., 12, 9775-9790, 10.5194/acp-12-9775-2012,
847 2012.
- 848 Smith, J. D., Kroll, J. H., Cappa, C. D., Che, D. L., Liu, C. L., Ahmed, M., Leone, S. R., Worsnop, D. R., and
849 Wilson, K. R.: The heterogeneous reaction of hydroxyl radicals with sub-micron squalane
850 particles: a model system for understanding the oxidative aging of ambient aerosols, Atmos.
851 Chem. Phys., 9, 3209-3222, 10.5194/acp-9-3209-2009, 2009.
- 852 Surratt, J. D., Chan, A. W. H., Eddingsaas, N. C., Chan, M., Loza, C. L., Kwan, A. J., Hersey, S. P., Flagan, R.
853 C., Wennberg, P. O., and Seinfeld, J. H.: Reactive intermediates revealed in secondary organic
854 aerosol formation from isoprene, Proc. Natl. Acad. Sci. USA, 107, 6640-6645,
855 10.1073/pnas.0911114107, 2010.
- 856 Tsigaridis, K., Daskalakis, N., Kanakidou, M., Adams, P. J., Artaxo, P., Bahadur, R., Balkanski, Y., Bauer, S.
857 E., Bellouin, N., Benedetti, A., Bergman, T., Berntsen, T. K., Beukes, J. P., Bian, H., Carslaw, K. S.,



- 858 Chin, M., Curci, G., Diehl, T., Easter, R. C., Ghan, S. J., Gong, S. L., Hodzic, A., Hoyle, C. R., Iversen,
859 T., Jathar, S., Jimenez, J. L., Kaiser, J. W., Kirkevåg, A., Koch, D., Kokkola, H., Lee, Y. H., Lin, G., Liu,
860 X., Luo, G., Ma, X., Mann, G. W., Mihalopoulos, N., Morcrette, J. J., Müller, J. F., Myhre, G.,
861 Myriokefalitakis, S., Ng, N. L., O'Donnell, D., Penner, J. E., Pozzoli, L., Pringle, K. J., Russell, L. M.,
862 Schulz, M., Sciare, J., Seland, Ø., Shindell, D. T., Sillman, S., Skeie, R. B., Spracklen, D., Stavrou,
863 T., Steenrod, S. D., Takemura, T., Tiitta, P., Tilmes, S., Tost, H., van Noije, T., van Zyl, P. G., von
864 Salzen, K., Yu, F., Wang, Z., Zaveri, R. A., Zhang, H., Zhang, K., Zhang, Q., and Zhang, X.: The
865 AeroCom evaluation and intercomparison of organic aerosol in global models, *Atmos. Chem.*
866 *Phys.*, 14, 10845-10895, 10.5194/acp-14-10845-2014, 2014.
- 867 Ulbrich, I. M., Canagaratna, M. R., Zhang, Q., Worsnop, D. R., and Jimenez, J. L.: Interpretation of organic
868 components from Positive Matrix Factorization of aerosol mass spectrometric data, *Atmos.*
869 *Chem. Phys.*, 9, 2891-2918, 2009.
- 870 Vaden, T. D., Imre, D., Beránek, J., Shrivastava, M., and Zelenyuk, A.: Evaporation kinetics and phase of
871 laboratory and ambient secondary organic aerosol, *Proc. Natl. Acad. Sci. USA*, 108, 2190-2195,
872 10.1073/pnas.1013391108, 2011.
- 873 Volkamer, R., Jimenez, J. L., San Martini, F., Dzepina, K., Zhang, Q., Salcedo, D., Molina, L. T., Worsnop, D.
874 R., and Molina, M. J.: Secondary organic aerosol formation from anthropogenic air pollution:
875 Rapid and higher than expected, *Geophys. Res. Lett.*, 33, Doi 10.1029/2006gl026899, 2006.
- 876 Washenfelder, R. A., Attwood, A. R., Brock, C. A., Guo, H., Xu, L., Weber, R. J., Ng, N. L., Allen, H. M.,
877 Ayres, B. R., Baumann, K., Cohen, R. C., Draper, D. C., Duffey, K. C., Edgerton, E., Fry, J. L., Hu, W.
878 W., Jimenez, J. L., Palm, B. B., Romer, P., Stone, E. A., Wooldridge, P. J., and Brown, S. S.:
879 Biomass burning dominates brown carbon absorption in the rural southeastern United States,
880 *Geophys. Res. Lett.*, 2014GL062444, 10.1002/2014gl062444, 2015.
- 881 Weitkamp, E. A., Lambe, A. T., Donahue, N. M., and Robinson, A. L.: Laboratory Measurements of the
882 Heterogeneous Oxidation of Condensed-Phase Organic Molecular Makers for Motor Vehicle
883 Exhaust, *Environ. Sci. Technol.*, 42, 7950-7956, 10.1021/es800745x, 2008.
- 884 Wong, J. P. S., Lee, A. K. Y., and Abbatt, J. P. D.: Impacts of Sulfate Seed Acidity and Water Content on
885 Isoprene Secondary Organic Aerosol Formation, *Environ. Sci. Technol.*,
886 10.1021/acs.est.5b02686, 2015.
- 887 Xie, Y., Paulot, F., Carter, W. P. L., Nolte, C. G., Luecken, D. J., Hutzell, W. T., Wennberg, P. O., Cohen, R.
888 C., and Pinder, R. W.: Understanding the impact of recent advances in isoprene photooxidation
889 on simulations of regional air quality, *Atmos. Chem. Phys.*, 13, 8439-8455, 10.5194/acp-13-8439-
890 2013, 2013.
- 891 Xu, L., Guo, H., Boyd, C. M., Klein, M., Bougiatioti, A., Cerully, K. M., Hite, J. R., Isaacman-VanWertz, G.,
892 Kreisberg, N. M., Knote, C., Olson, K., Koss, A., Goldstein, A. H., Hering, S. V., de Gouw, J.,
893 Baumann, K., Lee, S.-H., Nenes, A., Weber, R. J., and Ng, N. L.: Effects of anthropogenic
894 emissions on aerosol formation from isoprene and monoterpenes in the southeastern United
895 States, *Proc. Natl. Acad. Sci. USA*, 112, 37-42, 10.1073/pnas.1417609112, 2014.
- 896 Zhang, Q., Jimenez, J. L., Canagaratna, M. R., Allan, J. D., Coe, H., Ulbrich, I., Alfarra, M. R., Takami, A.,
897 Middlebrook, A. M., Sun, Y. L., Dzepina, K., Dunlea, E., Docherty, K., DeCarlo, P. F., Salcedo, D.,
898 Onasch, T., Jayne, J. T., Miyoshi, T., Shimonono, A., Hatakeyama, S., Takegawa, N., Kondo, Y.,
899 Schneider, J., Drewnick, F., Borrmann, S., Weimer, S., Demerjian, K., Williams, P., Bower, K.,
900 Bahreini, R., Cottrell, L., Griffin, R. J., Rautiainen, J., Sun, J. Y., Zhang, Y. M., and Worsnop, D. R.:
901 Ubiquity and dominance of oxygenated species in organic aerosols in anthropogenically-
902 influenced Northern Hemisphere midlatitudes, *Geophys. Res. Lett.*, 34, L13801, Doi
903 10.1029/2007gl029979, 2007.

904



905 **Table 1** Summary of k_{OH} , γ_{OH} and different experiment parameters used in this study and other
 906 lab studies.

Species Name	$k_{OH} \times 10^{12}$ (cm^3 $\text{molec.}^{-1} \text{s}^{-1}$)	γ_{OH}	OH conc.(molec. cm^{-3})	React. time	Particle Size (nm)	RH	Refer ences
IEPOX-SOA in SE US	0.40 ± 0.20	0.59 ± 0.33	$10^7 - 10^{10}$	~200s	415	~83%	(1)
IEPOX-SOA In SE US RH dependent	0.32	0.34	$10^7 - 10^{10}$	~200s	302	<60%	(1)
	0.33	0.39	$10^7 - 10^{10}$	~200s	328	60-80%	(1)
	0.34	0.46	$10^7 - 10^{10}$	~200s	380	80-90%	(1)
	0.64	1.19	$10^7 - 10^{10}$	~200s	525	90-100%	(1)
IEPOX-SOA in Amazon	0.39 ± 0.19	0.68 ± 0.38	$10^7 - 10^{10}$	~200s	490	~86%	(1)
IEPOX-SOA in Amazon RH dependent	0.35	0.45	$10^7 - 10^{10}$	~200s	363	<60%	(1)
	0.35	0.46	$10^7 - 10^{10}$	~200s	380	60-80%	(1)
	0.37	0.54	$10^7 - 10^{10}$	~200s	415	80-90%	(1)
	0.53	1.09	$10^7 - 10^{10}$	~200s	576	90%-100%	(1)
Highly oxidized organic species							
<i>BTA</i> ^a	0.76	0.51	$\sim 10^9 - 3 \times 10^{11}$	~37s	~130- 145	30%	(2)
<i>Citric acid</i>	0.43	0.37	$\sim 10^9 - 3 \times 10^{11}$	~37s	~130- 145	30%	(2)
<i>Tartaric acid</i>	0.33	0.40	$\sim 10^9 - 3 \times 10^{11}$	~37s	~130- 145	30%	(2)
<i>Erythritol</i>	0.25	0.77	$\sim 1 \times 10^9 - 2 \times 10^{11}$	~37s	~200	30%	(3)
Motor oil particles							
<i>Diesel particles</i>	0.4-34	0.1-8	$0.6 - 40 \times 10^6$	4h	~300	10-75%	(4)
<i>Nucleated motor oil particles</i>	N/A	0.72	$0 - 3 \times 10^{10}$	37s	~170	~30%	(5)
Biomass burning tracers							
<i>Levogluconan</i>	0.31	0.91	$\sim 1 \times 10^9 - 2 \times 10^{11}$	~37s	~200	30%	(3)
	0.14-0.43	0.21-0.65	10^8 to 10^9	N/A	120-267	0-40%	(6)
	N/A	0.15-0.6	$10^7 - 10^{11}$	<1 s	N/A	0%	(7)
<i>Abietic acid</i>	N/A	0.15-0.6	$10^7 - 10^{11}$	N/A	N/A	0%	(7)
<i>Nitroguaiacol</i>	N/A	0.2-0.5	$10^7 - 10^{11}$	N/A	N/A	0%	(7)
<i>MNC</i> ^b	0.04-0.16	0.07-0.22	10^8 to 10^9	N/A	203-307	0-26%	(6)
Other pure organic species							
<i>Squalene</i>	N/A	0.3 ± 0.07	1×10^{10}	~37s	~160	30%	(8)
<i>Squalene</i>	1.8-1.9	0.49-0.54	$1 - 7 \times 10^8$	1.5-3h	~220	30%	(9)
<i>Palmitic Acid</i>	N/A	0.8-1	$1.4 - 3 \times 10^{10}$	10-17s	85-220	~16%	(10)

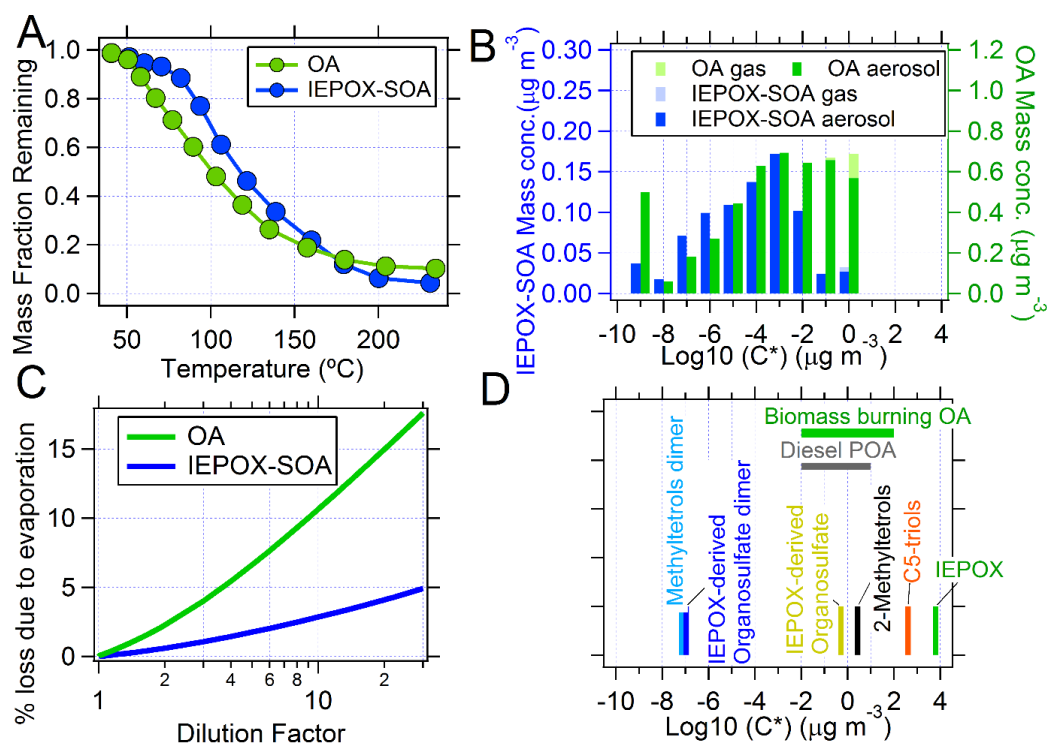
907 ^a 1, 2, 3, 4-Butanetetracarboxylic acid; ^b 4-methyl-5-Nitrocatechol

908 (1) This study; (2) (Kessler et al., 2012); (3) (Kessler et al., 2010); (4) (Weitkamp et al., 2008); (5) (Isaacman et al., 2012); (6)

909 (Slade and Knopf, 2014); (7) (Slade and Knopf, 2013); (8) (Smith et al., 2009); (9) (Che et al., 2009); (10) (McNeill et al., 2008).

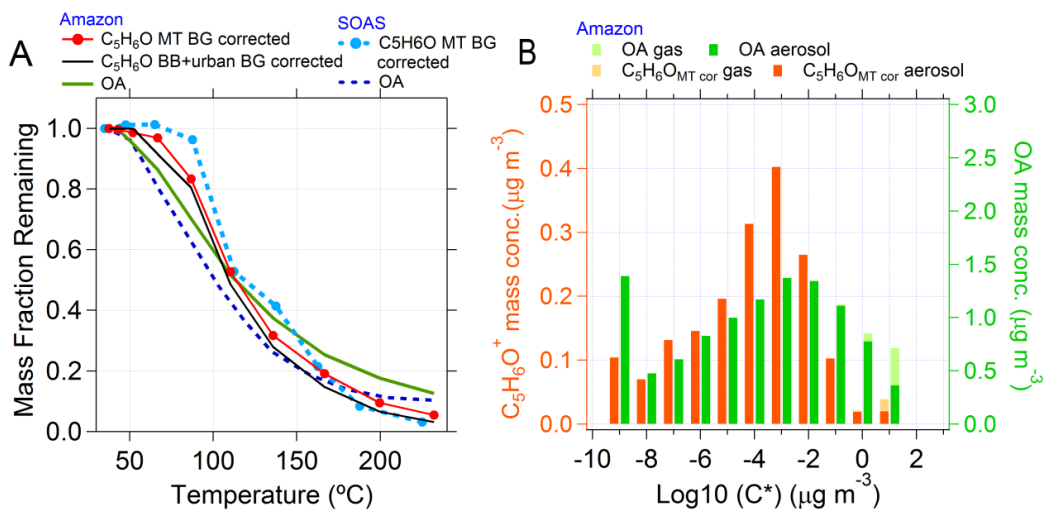


910



911

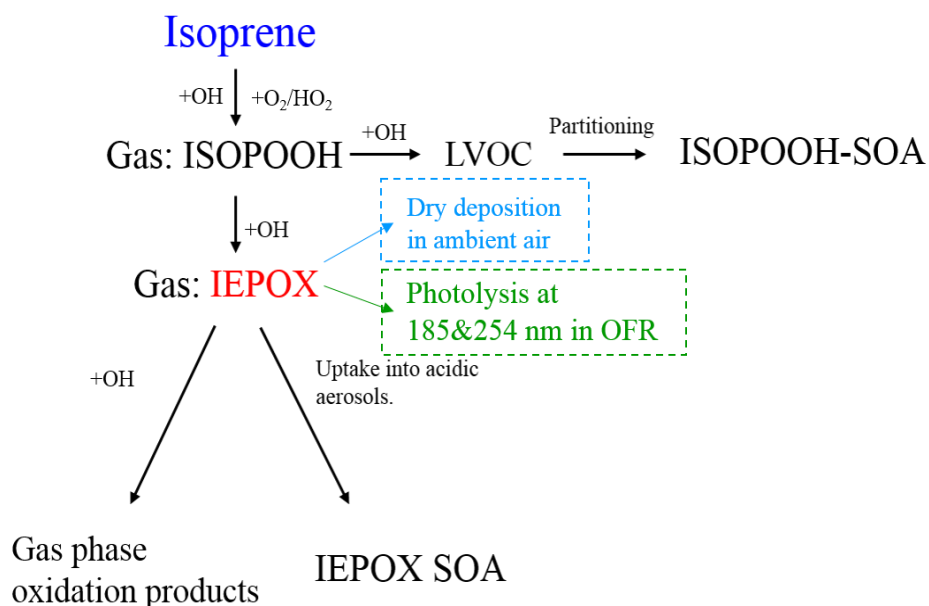
912 **Figure 1** (a) Mean mass fraction remaining of IEPOX-SOA and OA versus temperature in TD
 913 (“thermograms”) during SE US study. (b) Volatility distributions of IEPOX-SOA and OA
 914 estimated from TD thermograms (see text). Bars are offset for clarity and were both calculated
 915 for integer $\text{log}(C^*)$ values. (c) Evaporation losses of IEPOX-SOA and OA as a function of
 916 dilution factors. (d) Volatility of typical IEPOX-SOA molecular species in the aerosol phase
 917 based on the SIMPOL group contribution method (Pankow and Asher, 2008). The reduction in
 918 vapor pressure upon addition of a nitrate group was used to estimate the effect of the sulfate
 919 group, due to lack of SIMPOL parameters for the latter, and the derived C^* may be
 920 overestimated for this reason.



921

922 **Figure 2** (a) Thermogram of OA and background-corrected C₅H₆O⁺ ion in the SE US and
923 Amazon studies. (b) Volatility distributions of C₅H₆O⁺ and OA estimated based on TD
924 thermograms from the Amazon study.

925



926

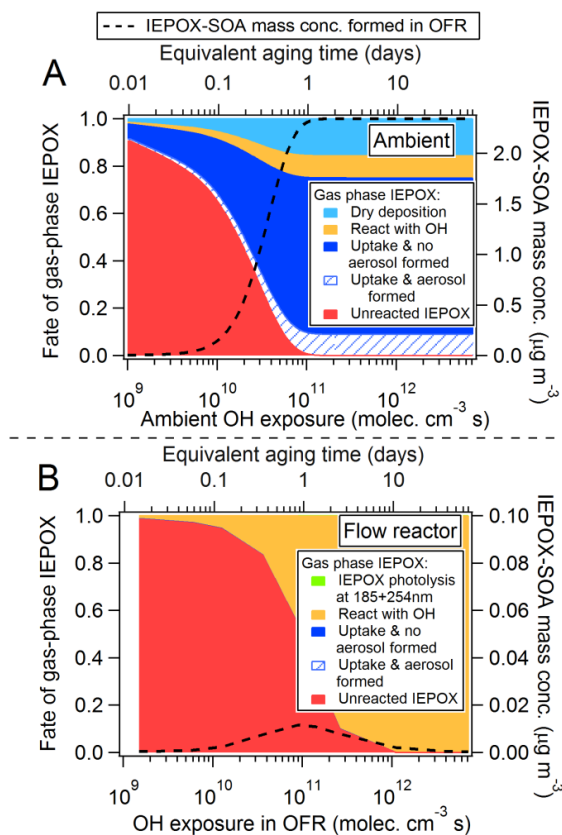
927 **Figure 3** Mechanism diagram of gas-phase IEPOX model in ambient and OFR conditions.
928 ISOPOOH-SOA is referred to SOA formed through gas-particle partitioning of low-volatile
929 VOCs from oxidation of isoprene 4-hydroxy-3-hydroperoxide (4,3-ISOPOOH) under low-NO
930 conditions (Krechmer et al., 2015).

931

932



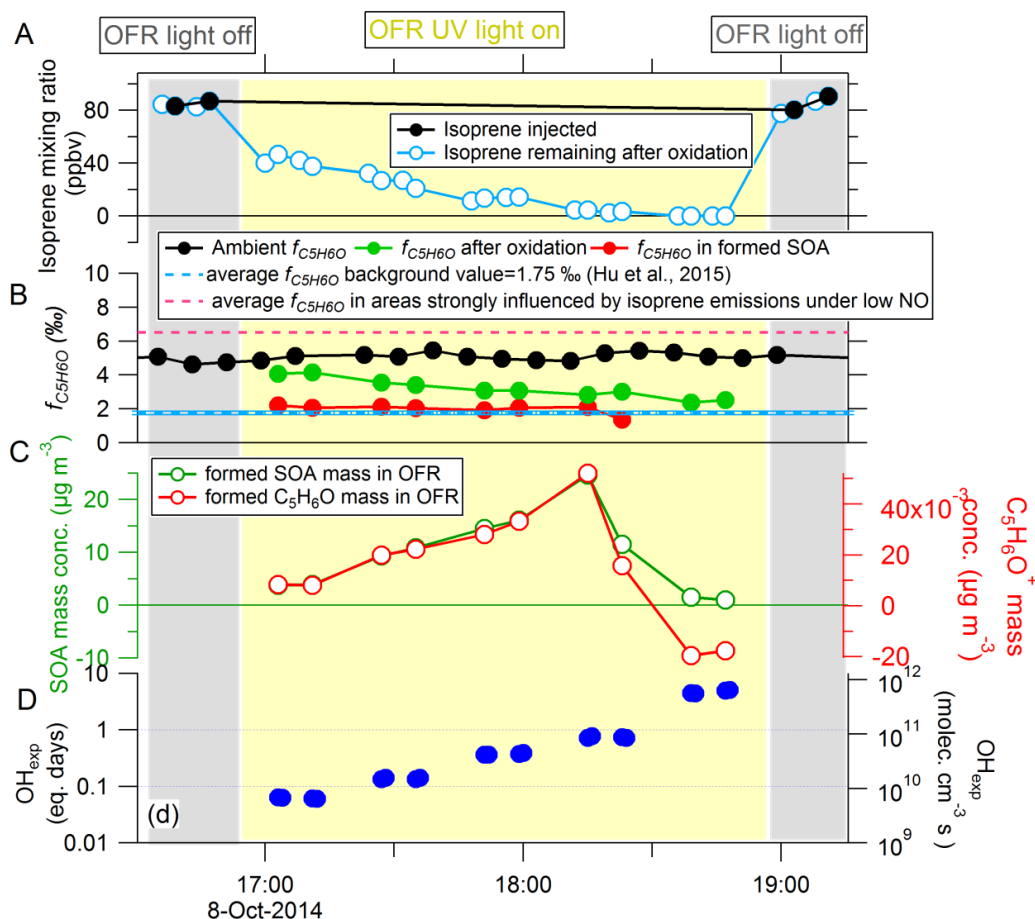
933



934

935 **Figure 4** Modeled IEPOX fate (a) in ambient air and (b) oxidation flow reactor (OFR)
936 conditions in SE US study. The uptake rate of gas-phase IEPOX onto aerosol is calculated by
937 using the model of Gaston et al. (2014), and is mainly influenced by aerosol pH (estimated as 0.8
938 and 1.35 for ambient and OFR aerosol, respectively) and aerosol surface areas (300 and 350
939 $\mu\text{m}^2/\text{cm}^3$ for ambient and OFR aerosol, respectively). The calculated IEPOX-SOA mass
940 concentrations are shown in Fig. 3. The OH exposures for both panels range 15 min-2 months of
941 atmospheric equivalent age (at OH concentration= 1.5×10^6 molec. cm^{-3}).

942

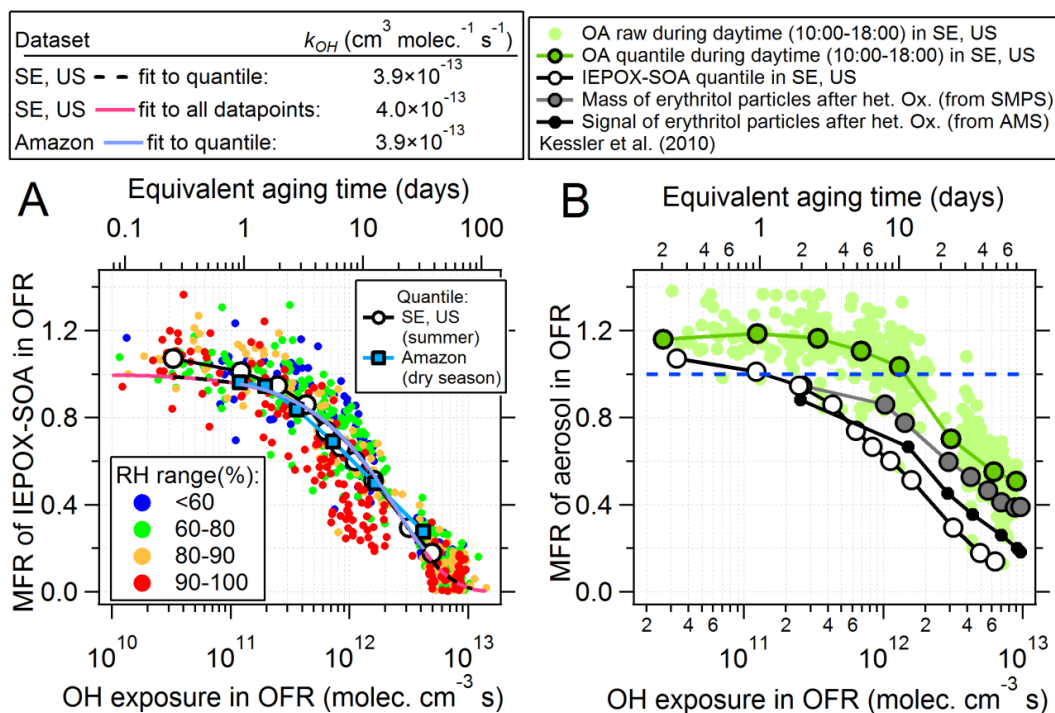


943

944 **Figure 5.** Isoprene standard addition experiment in ambient air during the GoAmazon2014/5
 945 study. (a) Isoprene concentration injected and remaining after OFR. (b) Time series of ambient
 946 $f_{C_5H_6O}$, $f_{C_5H_6O}$ in OA after oxidation and $f_{C_5H_6O}$ in newly formed SOA from OFR oxidation. The
 947 average background value $f_{C_5H_6O}=1.75\%$ from urban and biomass burning emissions and
 948 $f_{C_5H_6O}=6.5\%$ from aerosol strongly influenced by isoprene emissions are also shown (Hu et al.,
 949 2015). (c) Time series of mass concentration of newly formed SOA (left axis) and $C_5H_6O^+$ (right
 950 axis). (d) Time series of equivalent aging time (left axis) and OH exposure in OFR (right axis).
 951 OH concentration= 1.5×10^6 molec. cm^{-3} was assumed here to calculate equivalent OH aging
 952 times. The grey background indicates OFR light off period and light yellow is OFR light on
 953 period. Different OH exposures were achieved by varying the UV light intensity. Residence time
 954 in the OFR was about 200 s.



955



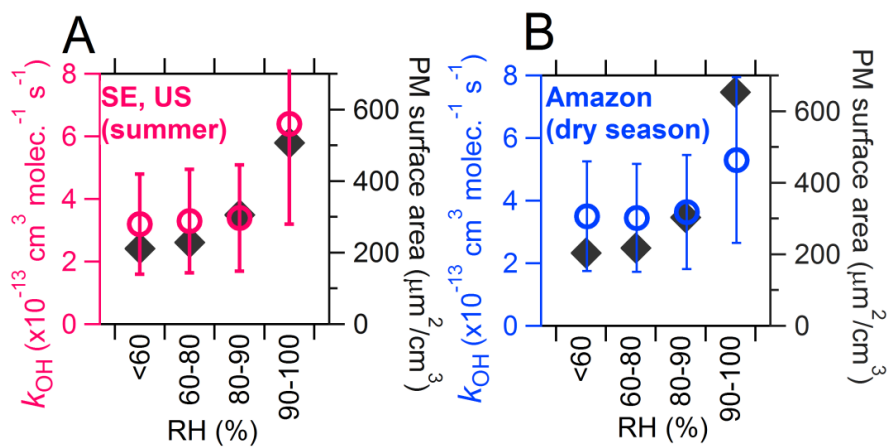
956

957 **Figure 6** (a) Mass fraction remaining (MFR) of IEPOX-SOA in OFR output as a function of OH
 958 exposure during the entire SOAS and GoAmazon 2014/5 (dry season) studies. Individual
 959 datapoints from SOAS are color-coded by ambient RH. Similar data for GoAmazon 2014/5 are
 960 shown in Fig. S24. (b) Mass fraction of OA remaining in OFR output as a function of OH
 961 exposure in daytime (12:00-18:00) during SOAS. Also shown is the MFR of pure erythritol
 962 particles after heterogenous oxidation as detected by SMPS and by AMS for reference (Kessler
 963 et al., 2010). Erythritol has a similar structure to the IEPOX-SOA tracers 2-methytetrols.

964



965



966

967

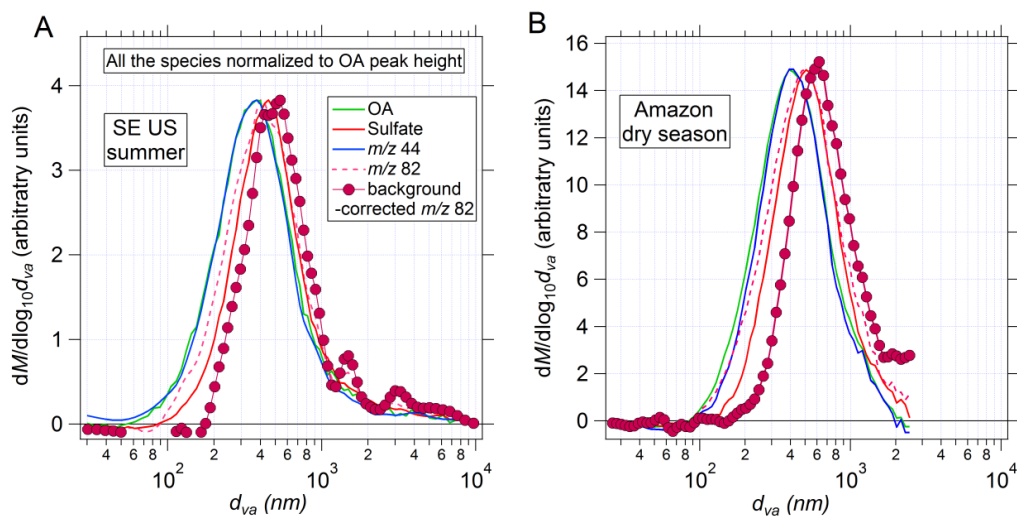
968 **Figure 7.** Estimated k_{OH} of IEPOX-SOA vs. ambient RH during the SOAS and Amazon studies.
969 The ambient wet particle surface areas in both studies are shown on the right axis.

970

971



972



973

974 **Figure 8.** Average mass-weighted aerodynamic size distribution of OA, sulfate, m/z 44 and m/z
975 82 in (a) SE US and (b) Amazon. The mass size distribution of m/z 82 with background
976 correction is also shown. The background correction method was introduced in Hu et al.(2015).
977 Heights of all the size distributions are set to the same value for ease of visual comparison.